FEASIBILITY STUDY OF A SYNTHESIS PROCEDURE FOR ARRAY FEEDS TO IMPROVE RADIATION PERFORMANCE OF LARGE DISTORTED REFLECTOR ANTENNAS

SEMIANNUAL STATUS REPORT

submitted to

NASA Langley Research Center

for

Grant No. NAG-1-859

by

W.L. Stutzman

K. Takamizawa

P. Werntz

J. LaPean

R. Barts

B. Shen

D. Dunn

Virginia Polytechnic Institute and State University

Bradley Department of Electrical Engineering

Blacksburg, Virginia 24061-0111

SATCOM Report No. 92-2

February 1992

TABLE OF CONTENTS

1. INTRODUCTION 4
2. PERFORMANCE ANALYSIS OF THE GREGORIAN TRI-REFLECTOR 7
2.1 Introduction 7
2.2 Primary Aperture Efficiency 9
2.3 Aperture Phase Errors 14
2.4 Conclusions 18
2.5 Recommendations for Future Work 18
2.6 References 18
3. DESIGN AND PERFORMANCE OF THE TYPE 6 REFLECTOR ANTENNA 19
3.1 The Type 6 Concept 19
3.2 Dual-Reflector Antenna Synthesis (DRAS30) Coding Approach 19
3.3 Electromagnetic Analysis Results - Nominal Case 26
3.4 Three Dimensional Mizugutch Condition - Electromagnetics Analysis Results 26
4. A NEW SPHERICAL MAIN REFLECTOR SYSTEM DESIGN. 50
4.1 Introduction 50
4.2 An Overview of Our New Approach. 50
4.3 Summary of Three Motions. 52
4.4 Test Cases 52
5. OPTIMIZATION OF REFLECTOR CONFIGURATIONS USING PHYSICAL OPTICS 55
5.1 Introduction 55
5.2 Optimization of Foldes Type 6 Configuration 56
5.3 Application of PO Optimization 58
5.4 Conclusions and Future Work 62
5.5 References 62
6. RADIOMETRIC ARRAY DESIGN 65
7. BEAM EFFICIENCY STUDIES 66
8. PUBLICATIONS 66
8.1 Recent Publications 66
8.1.1 Conferences 66
8.1.2 Papers. 66
8.1.3 Theses, Dissertations, Reports. 67
8.2 Planned Publications 67
8.2.1 Conferences 67

8.2.2 Papers. 67
8.2.3 Theses, Dissertations, Reports. 67

1. INTRODUCTION

Virginia Tech is involved in a number of activities with NASA Langley related to large aperture radiometric antenna systems. These efforts are summarized in Table 1-1. This semi-annual report is primarily directed toward the grant first listed in Table 1-1; however, some results for all activities are reported here as well. Table 1-2 lists the major reflector antenna research areas together with the students performing the work.

Table 1-1

REFLECTOR ANTENNA RESEARCH AT VIRGINIA TECH

1. "Feasibility Study of a Synthesis Procedure for Array Feeds to Improve Radiation Performance of Large Distorted Reflector Antennas"

   GAs: Ko Takamizawa, Jim LaPean, Paul Werntz

   Project: NASA Grant NAG-1-859; VT 4-26132

   Term: 02/25/88 - 12/31/91

2. "Design of Array Feeds for Large Reflector Antennas"

   GA: Mike Barts

   Project: NASA Graduate Student Researchers Program: NGT-50413; VT 4-26204

   Term: 08/16/89 - 08/15/92

PERSONNEL ACTIVE IN REFLECTORS BUT NOT SUPPORTED BY NASA

3. Bing Shen, Ph.D. student

   Dissertation topic: Reflector Antenna Synthesis with Application to Scanning Systems with Spherical or Shaped Main Reflectors

4. Derrick Dunn, M.S. student

   Support: GEM Fellowship (6/91 to 12/92); NASA Traineeship (1/93 -)

Table 1-2

REFLECTOR ANTENNA RESEARCH ACTIVITIES AT VIRGINIA TECH

I. Technology Development

1.1. Operation and testing of full commercial reflector code (GRASP7) - Takamizawa

1.2. Multiple reflector cylindrical antenna code (MRAPCA) - Takamizawa

1.3. Documentation of analysis techniques for reflector computations - Takamizawa

1.4. Canonical cases - Dunn

1.5. Beam efficiency studies - Dunn

II. Wide Scanning Antenna Systems

2.1. Documentation of wide scanning antenna principles - Werntz

2.2. Type 2 tri-reflector antenna design - Werntz

2.3. Type 6 dual-reflector design - LaPean

2.4. Support of Type 6 hardware model - LaPean and Werntz

2.5. Spherical reflector antenna designs - Shen

2.6. Other concepts

Cylindrical reflector family

Toroidal reflector family

Hybrid concepts

III. Reflector System Optimization - Takamizawa

3.1 Comparison of optimization techniques

3.2 Application of optimization using PO

3.3 Error functional definition

IV. Arrays for Large Radiometric Antennas - Barts

4.1. Analysis techniques in lossy radiometric systems using arrays.

4.2. Feed array architectures for radiometers

4.3. Feed component technology readiness evaluation

4.4. Calibration issues

4.5. Beam efficiency studies

2. PERFORMANCE ANALYSIS OF THE GREGORIAN TRI-REFLECTOR

Preliminary performance results for a three-dimensional configuration designed to be compatible with the main reflector dimensions of the NASA Langley test article are presented. The Gregorian tri-reflector configuration was synthesized using the geometrical optics code TRAS-3D (Tri-Reflector Antenna Synthesis 3-Dimensional). All performance results were obtained from GRASP7 computations. The following two performance criteria were of primary importance: primary aperture efficiency and scan induced aperture phase errors.

2.1 Introduction

The reflector antenna configuration discussed in this section is derived from the reflector configuration originally proposed by Foldes [1]. This reflector configuration allows beam scanning with a minimum of subreflector motion and no feed motion. The reflector configuration is shown in Fig. 2-1. The main reflector diameter is 10.7 m with a focal length of 13.1 m and a center offset of 7.75 m. The subreflector diameter is ~ 5 m and the tertiary diameter is ~ 2.3 m. The parent focal length-to-diameter-ratio for this configuration is approximately $F/D_p = 0.5$. This small value limits scan performance. The feed in Fig. 2-1 is represented by a center point and a line. The center point indicates the system focal point for boresight operation. The line represents an array feed and shows the size and location of a 13 element feed array with interelement spacings of 0.09 m (1.5 λ at 5.0 GHz).

The beam scanning range of the configuration shown in Fig. 2-1 is a 5° angular cone about the boresight direction (which is parallel to the z-axis). In the following the vector representing the beam scan direction is given by the angles θ and ϕ, where θ is the angle between the scan vector and the z-axis and ϕ is the angle between the xy-plane projection of the scan vector and the x-axis.

The tertiary reflector is shaped to produce zero phase errors in the aperture plane for the boresight scan direction. Scanning is accomplished by tertiary rotation about a central point on its surface. The required motion of the tertiary for a given scan direction is calculated by TRAS-3D which uses Powell's optimization method. The error function used in the optimization is

$$E = \sum_{i=0}^{M} \sum_{j=0}^{N} w(i,j) \, |\hat{t}_{ij} \times \hat{s}| \qquad (2\text{-}1)$$

where $\hat{t}_{ij}$ is the unit vector in the direction of the i,j^{th} transmitted ray, $\hat{s}$ is the unit vector in the desired scan direction and $w(i,j)$ is the weighting of the i,j^{th} transmitted ray at the aperture plane as result of a cos^q feed distribution. This error function minimizes the divergence of the transmitted ray from the desired scan direction and therefore minimizes the aperture phase error.

2.2 Primary Aperture Efficiency

If phase errors are ignored, the primary aperture efficiency is affected by spillover at the surfaces of the primary, secondary and tertiary reflectors and the aperture taper efficiency, which lead to gain loss relative to a uniformly illuminated aperture due to the design aperture distribution. The primary aperture efficiency is calculated by the following expression [1]:

$$\eta = \frac{\left(\int\int_{-\infty}^{\infty} fg \, dx \, dy \right)^2}{\int\int_{-\infty}^{\infty} f^2 \, dx \, dy \int\int_{-\infty}^{\infty} g^2 \, dx \, dy} \tag{2-2}$$

where the integrals are evaluated over the aperture of the primary reflector, f is the field amplitude across the aperture due to an incident plane wave and g is the field amplitude across the aperture due to the feed excitation. As formulated, (2-2) includes both aperture taper and spillover effects.

The aperture field amplitude distribution due to the feed excitation can be found by ray tracing from the feed to the aperture plane. The geometrical optics boundary of the aperture illumination can be found by the locus of rays which when traced from the feed to the primary aperture intercept the edge of the tertiary. Figure 2-2 shows the geometric optics boundary of aperture illumination for scan directions of $\theta = 5^\circ$ and $\phi = 0^\circ$, 45°, 90°, 135° and 180°. These illuminations were calculated for a 2.3 m diameter tertiary for which the geometrical optics boundary of aperture illumination for boresight operation corresponds to the rim of the main reflector. The solid line in Fig. 2-2 represents the rim of the primary reflector. Figure 2-2 demonstrates a large amount of main reflector underillumination in the $\phi = 0^\circ$ and $\phi = 45^\circ$ scan directions, and main reflector spillover in the $\phi = 135^\circ$ and $\phi = 180^\circ$ scan directions. Main reflector spillover can be corrected by the use of an array feed, however, main reflector underillumination is caused by tertiary spillover and can only be corrected by increasing the size of the tertiary reflector. Aperture efficiency was calculated using (2-2) in order to assess the effects of the changing aperture illumination. For these calculations a single feed with a $cos^q \theta$ amplitude distribution and q chosen to give a -15 dB tertiary edge illumination for boresight operation was used. The results of these efficiency calculations are shown in Fig. 2-3.

To reduce the amount of tertiary spillover, the tertiary diameter was increased by 25 % to 2.87 m. The geometrical optics boundaries of primary aperture illumination corresponding to the enlarged tertiary for scan directions of $\theta = 5^\circ$ and $\phi = 0^\circ$, 45°, 90°, 135° and 180° are shown in Fig 2-4. The figure indicates that for this case main reflector under illumination is almost eliminated. The results of efficiency calculations for a fixed feed with a $cos^q \theta$ amplitude distribution and q chosen to give a -15

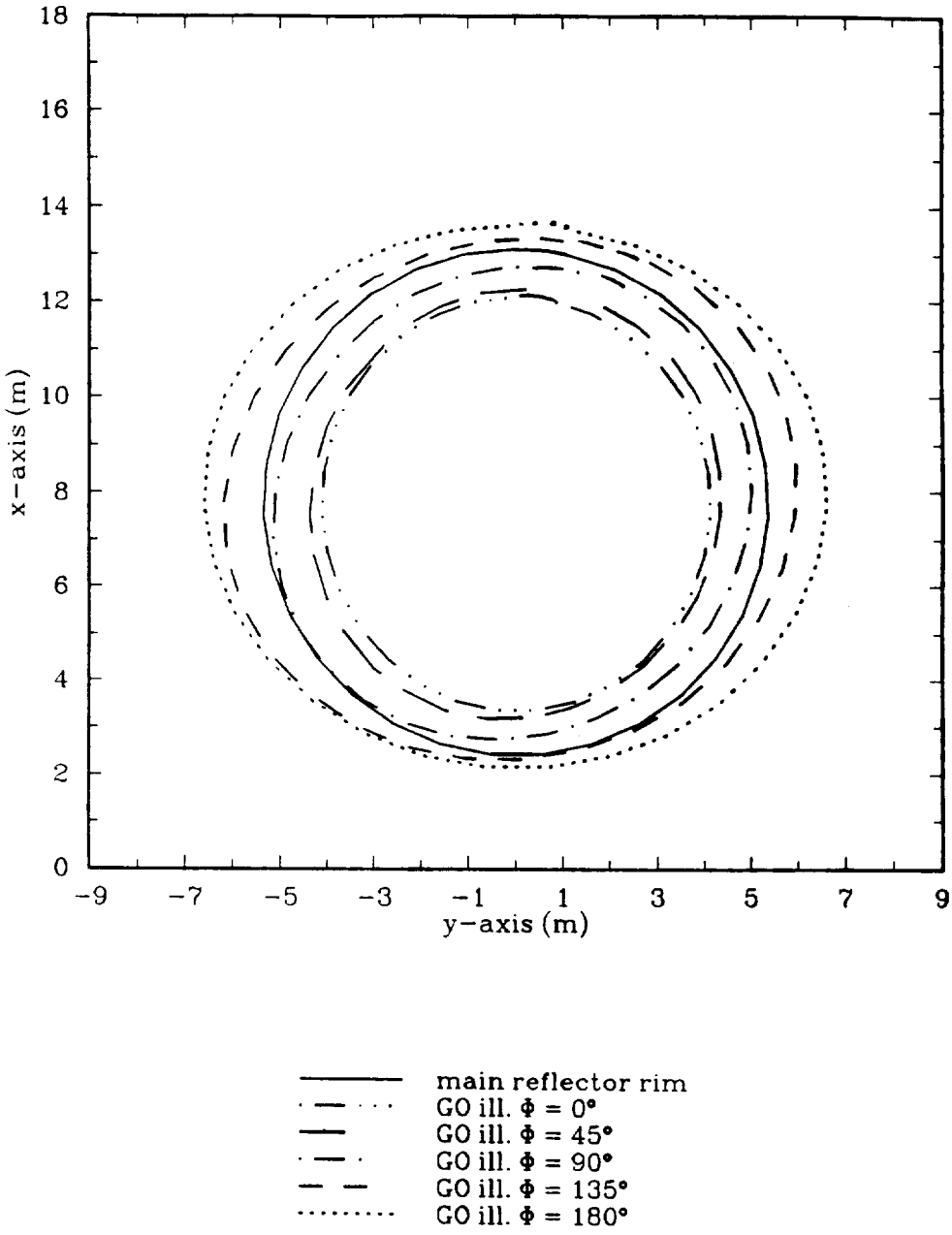

Figure 2-2. Geometrical optics boundary of aperture illumination corresponding to a 2.3 m tertiary for scan directions of $\theta = 5^{\circ}$ and $\phi = 0^{\circ}$, 45°, 90°, 135° and 180°. The solid line represents the rim of the main reflector.

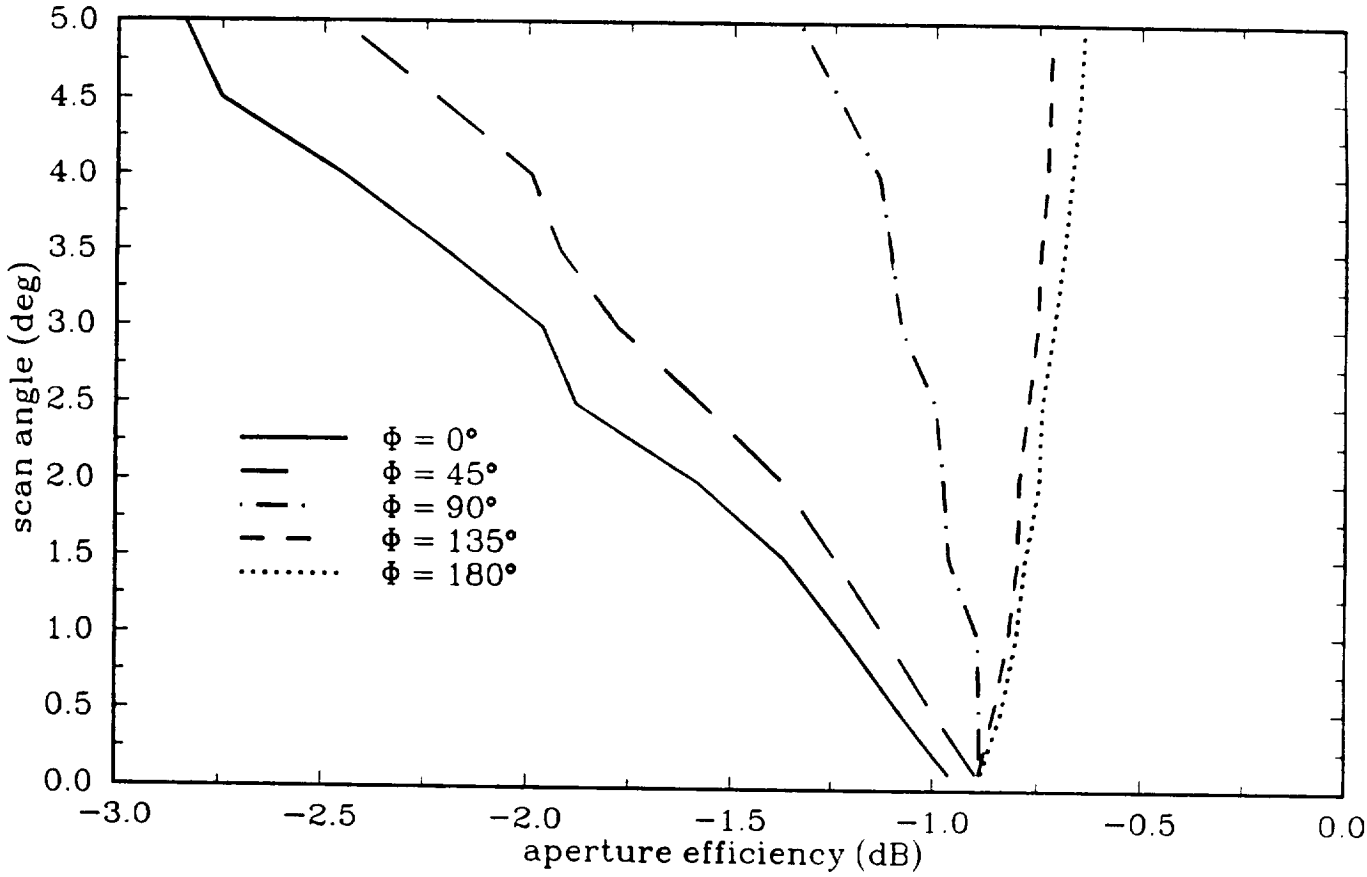

Figure 2-3. Aperture efficiency as a function scan angle for the Gregorian tri-reflector with a 2.3 m tertiary. Results are shown for scan angles of $\theta = 0°$ to 5°, and $\phi = 0°$, 45°, 90°, 135° and 180°.

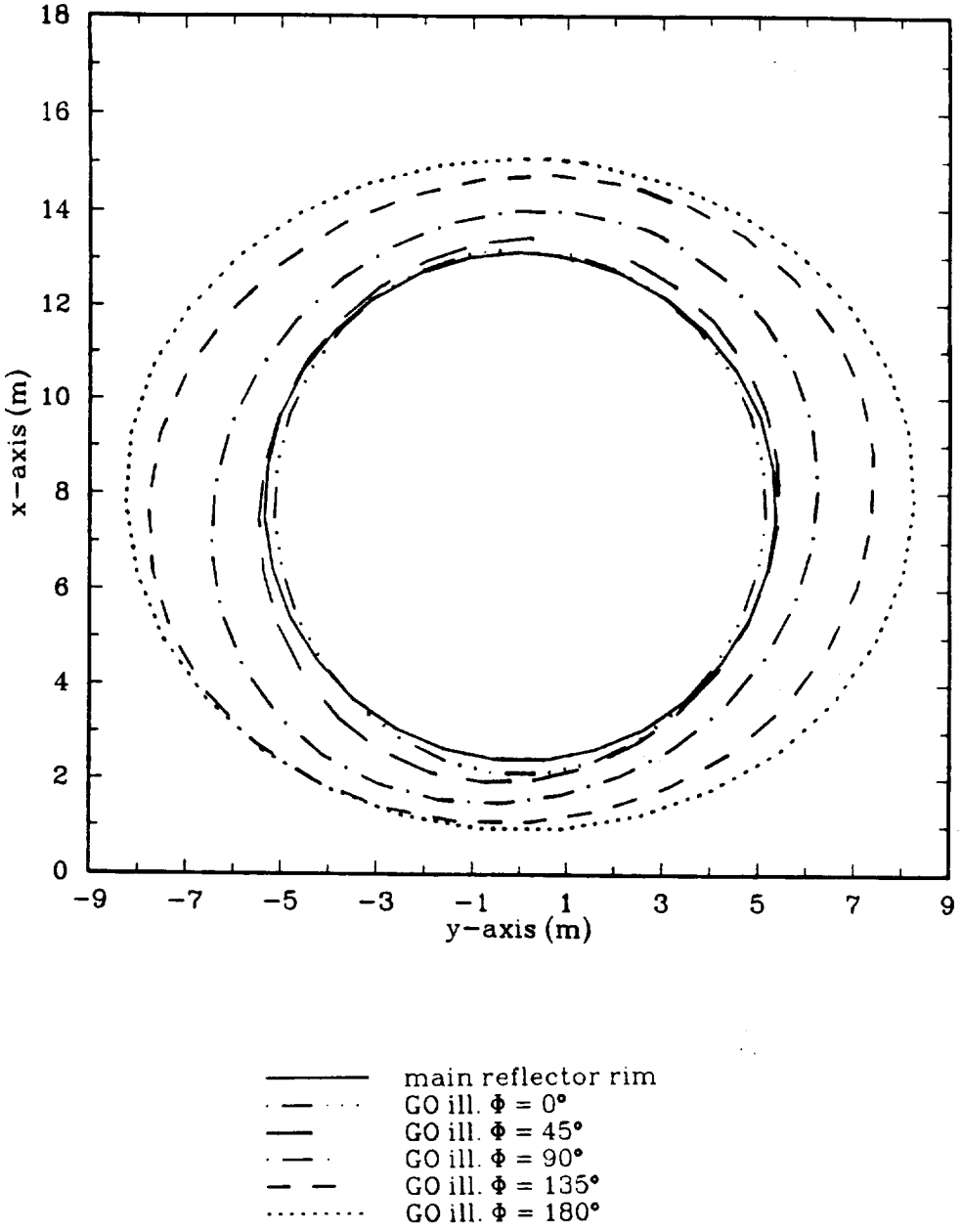

Figure 2-4. Geometrical optics boundary of aperture illumination corresponding to a 2.87 m tertiary for scan directions of $\theta = 5^{\circ}$ and $\phi = 0^{\circ}$, 45°, 90°, 135° and 180°. The solid line represents the rim of the main reflector.

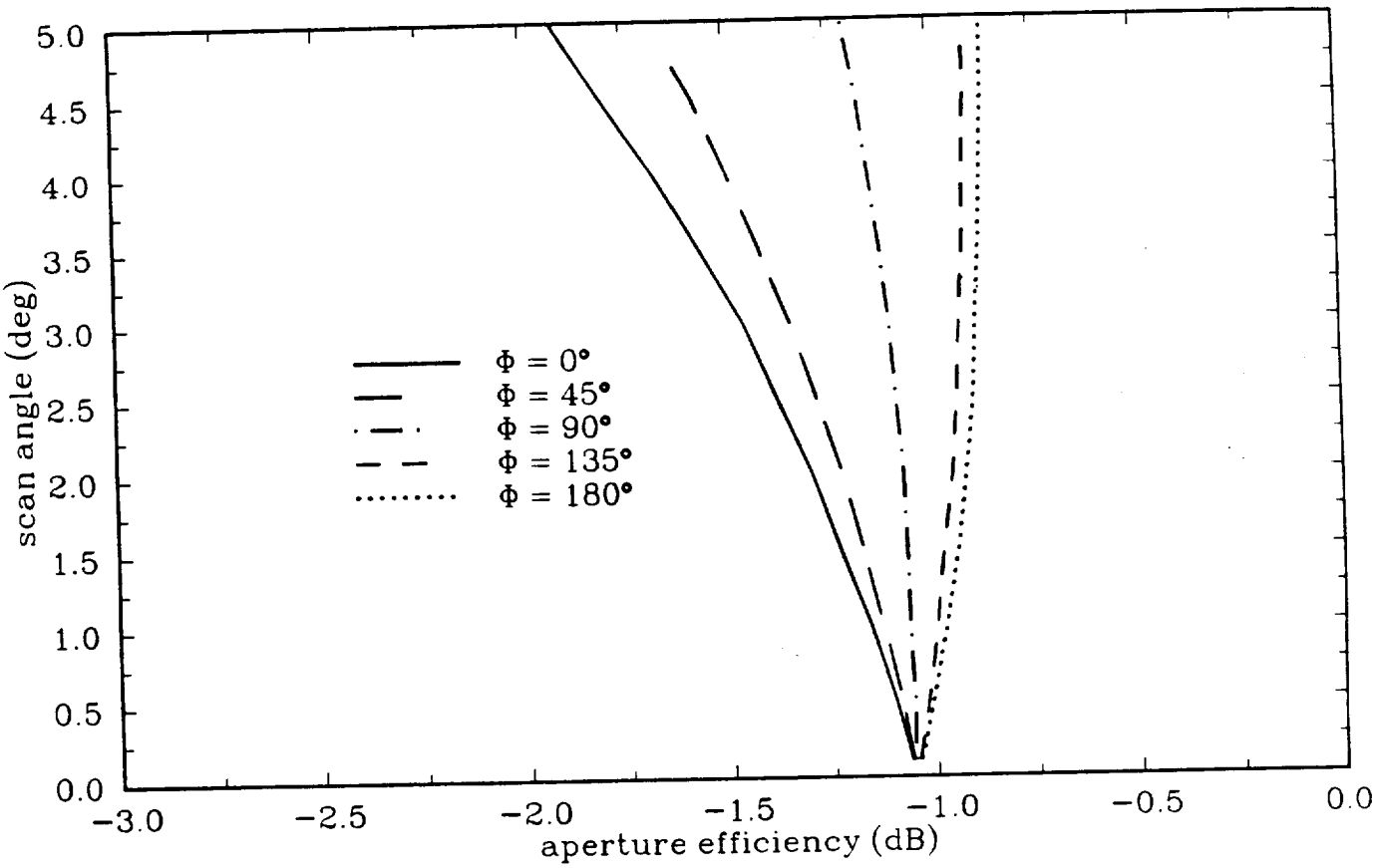

Figure 2-5. Aperture efficiency as a function scan angle for the Gregorian tri-reflector with a 2.87 m tertiary. Results are shown for scan angles of $\theta = 0^{\circ}$ to 5°, and $\phi = 0^{\circ}$, 45°, 90°, 135° and 180°.

dB edge illumination on the enlarged tertiary are shown in Fig. 2-5. Figure 2-5 indicates that efficiency loss in the $\phi = 0^{\circ}$ and $\phi = 45^{\circ}$ scan directions has been greatly reduced. The remaining efficiency loss is due to the aperture taper and can be corrected by an array feed.

2.3 Aperture Phase Errors

For a given *rms* phase error across the primary aperture, Φ_{rms}, the Ruze approximation can be used to derive the following useful equation which relates the main reflector diameter in wavelengths, D/λ, to the maximum allowed gain loss, G/G_0 [2]:

$$\frac{D}{\lambda} = \left\{ \frac{1 - G/G_0}{(\frac{\pi}{r})^2 \Phi_{rms}} \right\}^{1/2} \tag{2-3}$$

where r is the radius of the primary aperture. In the following examples the maximum allowed gain loss was chosen to be -1 dB ($G/G_0 = 0.7943$). The following three configurations were evaluated: the Gregorian tri-reflector with a 2.3 m tertiary, the Gregorian tri-reflector with a 2.87 m tertiary and an offset prime focus reflector system. The reflector used in the prime focus configuration was identical to the main reflector used in the tri-reflector configurations. The feed motion for scanning the prime focus reflector configuration was calculated using the same optimization routine used to calculate the tertiary motions in the tri-reflector configurations, however, feed motion was unrestricted resulting in complex feed motions with large translational movement. The feeds used for the tri-reflector configurations were designed to provide a -15 dB tertiary edge illumination for boresight operation. The feed used for the prime focus reflector configuration was designed to provide a -15 dB main reflector edge illumination. Results of these calculations are shown in Figs. 2-6 to 2-8. Figures 2-6 and 2-7 show the results for the two tri-reflector configurations. These figures indicate that increasing the tertiary from 2.3 m to 2.87 m has little effect on phase error performance. Figure 2-8 shows the results for the prime focus parabolic reflector. For the prime-focus configuration, the values of D/λ are not as strongly dependent on the ϕ-scan direction as for the tri-reflector configurations. Comparison of Figs. 2-6 and 2-7 with Fig. 2-8 indicate that the performance of the tri-reflectors bracket that of the prime-focus parabolic reflector. For $\phi = 90^{\circ}$ (scanning orthogonal to the plane of symmetry) the tri-reflector diameter D/λ is approximately twice that for the prime-focus configuration while for $\phi = 0^{\circ}$ (scanning in the plane of symmetry), the tri-reflector diameter D/λ is approximately half that for the prime-focus configuration. The degraded scan performance of the tri-reflector configuration in the plane of symmetry compared to the prime focus configuration is due to even order phase errors introduced by the elliptic subreflector. Phase errors can be reduced and scan performance can be improved by allowing limited tertiary translation.

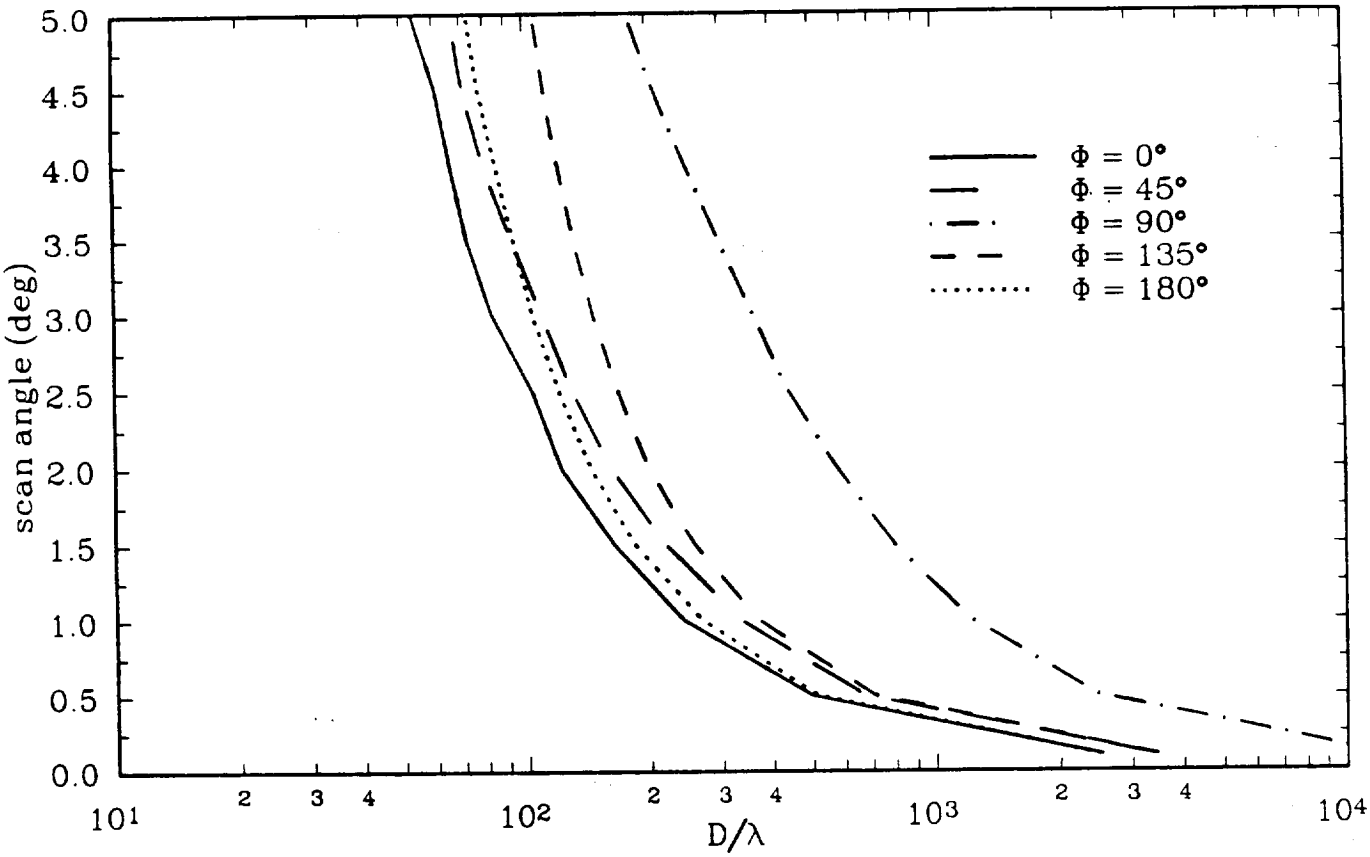

Figure 2-6. Scan performance of the Gregorian tri-reflector with a 2.3 m tertiary. Scan induced phase error is expressed as maximum main reflector D/λ for -1 dB gain loss. Results shown for scan angles of $\theta = 0^{\circ}$ to 5°, and $\phi = 0^{\circ}$, 45°, 90°, 135° and 180°.

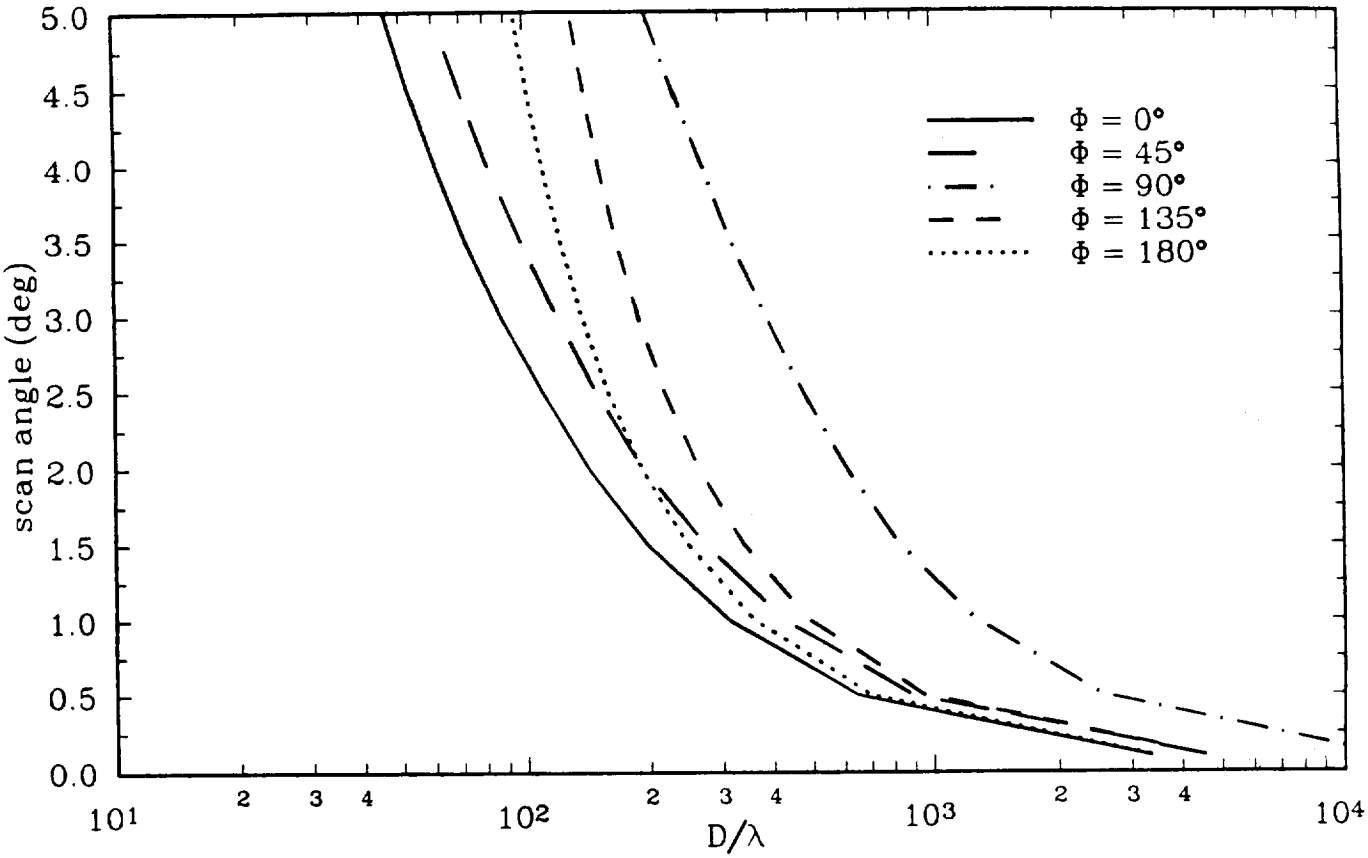

Figure 2-7. Scan performance of the Gregorian tri-reflector with a 2.87 m tertiary. Scan induced phase error is expressed as maximum main reflector D/λ for -1 dB gain loss. Results shown for scan angles of $\theta = 0°$ to 5°, and $\phi = 0°$, 45°, 90°, 135° and 180°.

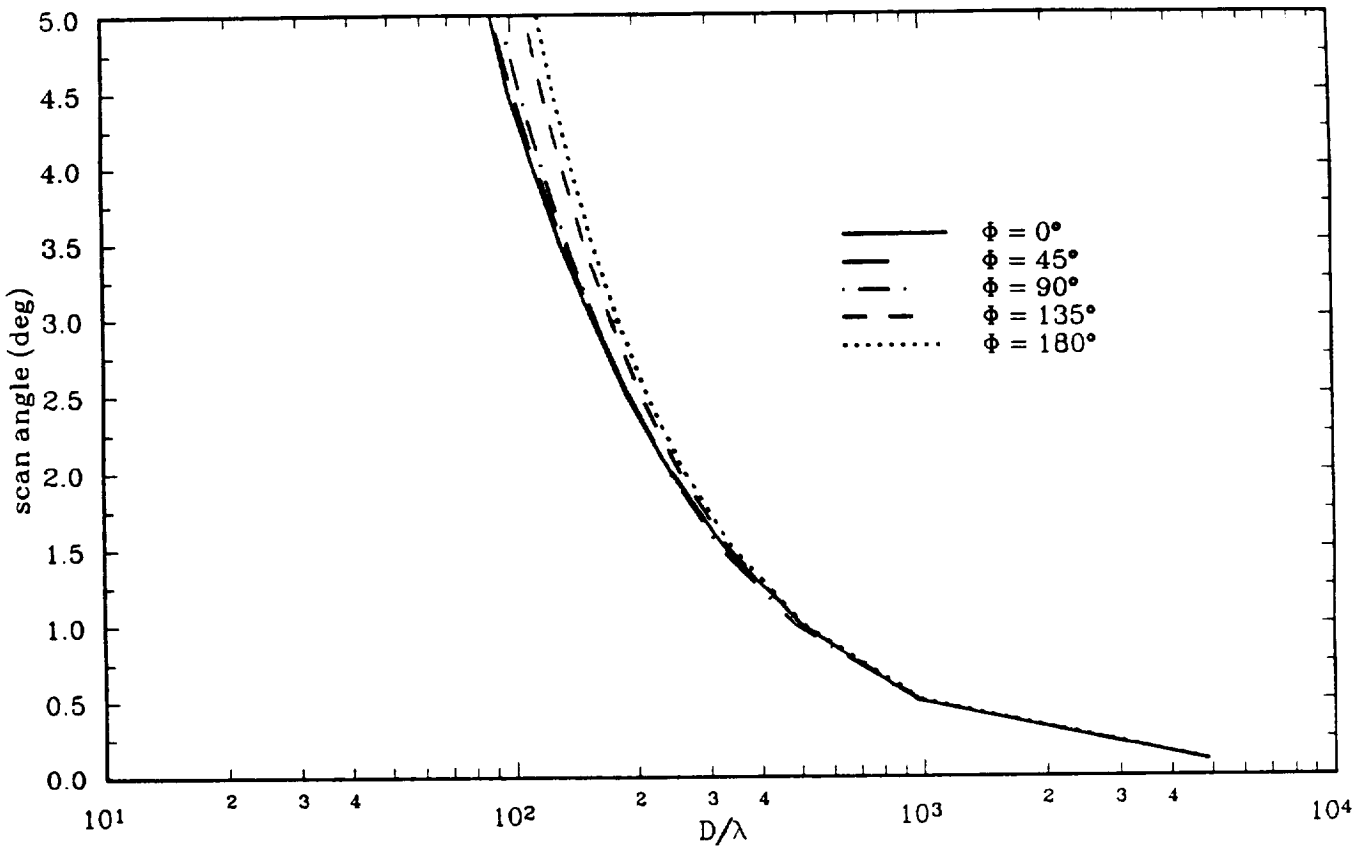

Figure 2-8. Scan performance of the prime-focus parabolic reflector. Scan-induced phase error is expressed as maximum main reflector D/λ for -1 dB gain loss. Results shown for scan angles of $\theta = 0°$ to 5°, and $\phi = 0°$, 45°, 90°, 135° and 180°.

2.4 Conclusions

(1) The Gregorian tri-reflector illumination efficiency was investigated. To prevent under illumination of the main reflector, it was found that the tertiary diameter must be increased by approximately 25% compared to the tertiary diameter which gives full main reflector illumination for boresight operation.

(2) The scan performance of the Gregorian tri-reflector, in terms of aperture plane phase errors, was compared to that of a prime-focus parabolic reflector. Compared to the prime-focus configuration the tri-reflector exhibits enhanced scan performance in the plane of symmetry and degraded performance perpendicular to the plane of symmetry.

2.5 Recommendations for Future Work

Future work will include:

(1) Tertiary translation in the previously investigated configurations.

(2) Investigate the effects of main reflector F/D ratio.

(3) Investigation array feed Gregorian tri-reflector scan performance.

2.6 References

[1] P. Foldes, Foldes Inc., 1131 Radnor Hill Road, Wayne, PA 19087.

[2] C. Dragone, M. J. Gans, "Imaging Reflector Arrangements to Form a Scanning Beam Using a Small Array," *Bell Systems Tech. Journal*, Vol. 58, no. 2, pp. 501-515, February 1979.

[3] A. V. Mystik, P. G. Smith, "Scanning Capabilities of Large Parabolic Cylinder Reflector Antennas with Phased-Array Feeds," *IEEE Trans. Ant. Prop.*, Vol. AP-29, no. 3, pp 455-462, May 1981.

3. DESIGN AND PERFORMANCE OF THE TYPE 6 REFLECTOR ANTENNA

The Type 6 reflector antenna system as first proposed by Peter Foldes is discussed in this section. The dimensions used are those for the original geometry. The three-dimensional antenna synthesis procedure is presented. Electromagnetics analysis results are shown for the original geometry and a modified geometry which satisfies the Mizugutch minimum cross-polarization condition.

3.1 The Type 6 Concept

The Type 6 antenna system is an offset Cassegrain dual-reflector antenna. This system has a design scan range of $\pm 0.5^{\circ}$. This configuration is designed to scan by subreflector motion only to minimize the moving mass of the system. The combination of a dual-offset design and the small subreflector also reduces aperture blockage and allows a longer electrical focal length for a given mechanical size. The overall dimensions of the Type 6 antenna are shown in Fig. 3.1-1. Three dimensional views of the antenna system are shown in Fig. 3.1-2 (a-d). The scan angle from the +z-axis is θ and the scan angle in the xy-plane from the x-axis towards the y-axis is ϕ.

3.2 Dual-Reflector Antenna Synthesis - 3 Dimensional (DRAS-3D)

The three dimensional synthesis of the Type 6 reflector antenna system was performed using DRAS-3D code. This program uses geometric optics techniques to determine the optimal subreflector position for an unscanned subreflector in the scanned system. The unscanned subreflector is allowed to be translated in three dimensions and rotated in two directions. The error function used in the optimization is

$$E = \sum_{i=1}^{M} \sum_{j=1}^{N} | \overline{t}_{ij} \times \overline{s} |^2 \qquad (3\text{-}1)$$

where $\overrightarrow{t}_{ij}$ is a unit vector in the direction of the i,jth transmitted ray and $\overline{s}$ is a unit vector in the desired direction of scan. This error function minimizes the divergence of the transmitted rays from the scan direction and therefore minimizes the aperture phase error.

This error function was found to perform much better than the previously-used Kitsuregawa error method which attempts to fit the unscanned subreflector to a correcting subreflector for each direction of scan. The relative subreflector positions for each method are shown in Fig. 3.2-1. While the Kitsuregawa fitting method provides a more even aperture illumination, the aperture phase error optimization method greatly increases scanned antenna performance by reducing phase errors. The aperture phase error method could be further improved by including a measure of the aperture illumination and spillover efficiency in the error functional.

After the optimal position of the subreflector in the scanned system is determined, the

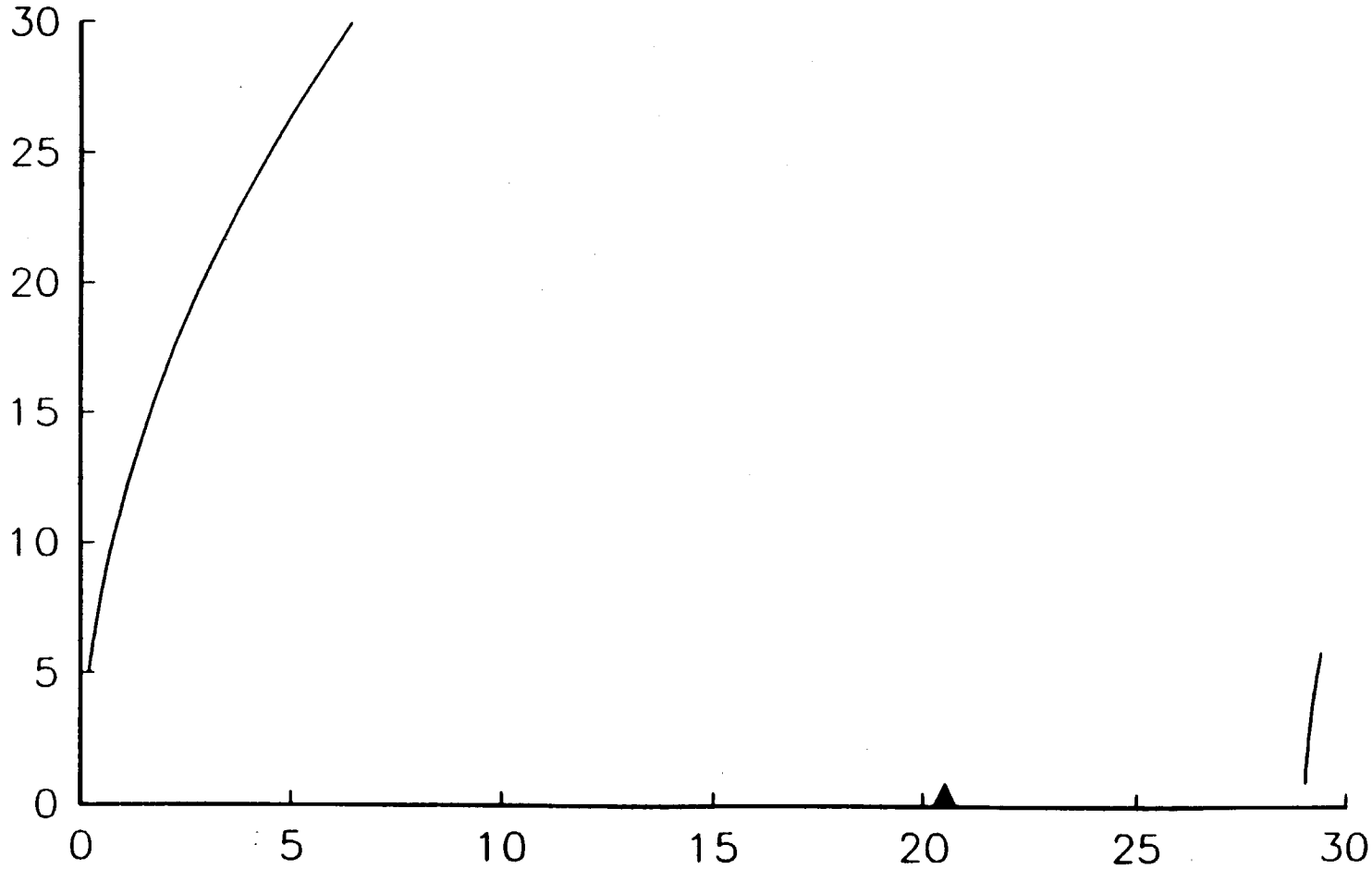

Figure 3.1-1. Type 6 reflector antenna system (profile view).

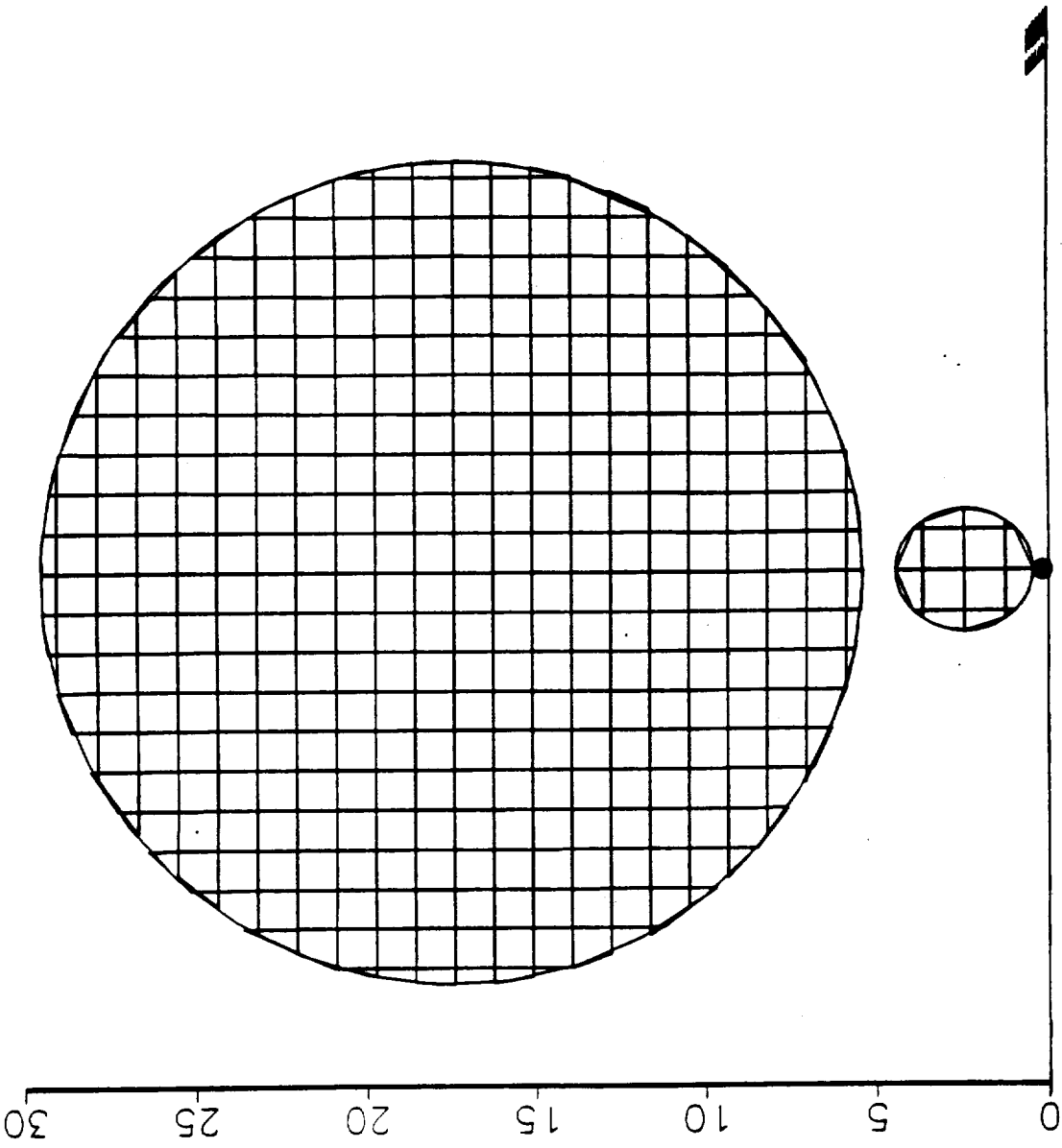

Figure 3.1-2 (a). Type 6 reflector antenna system (front view).

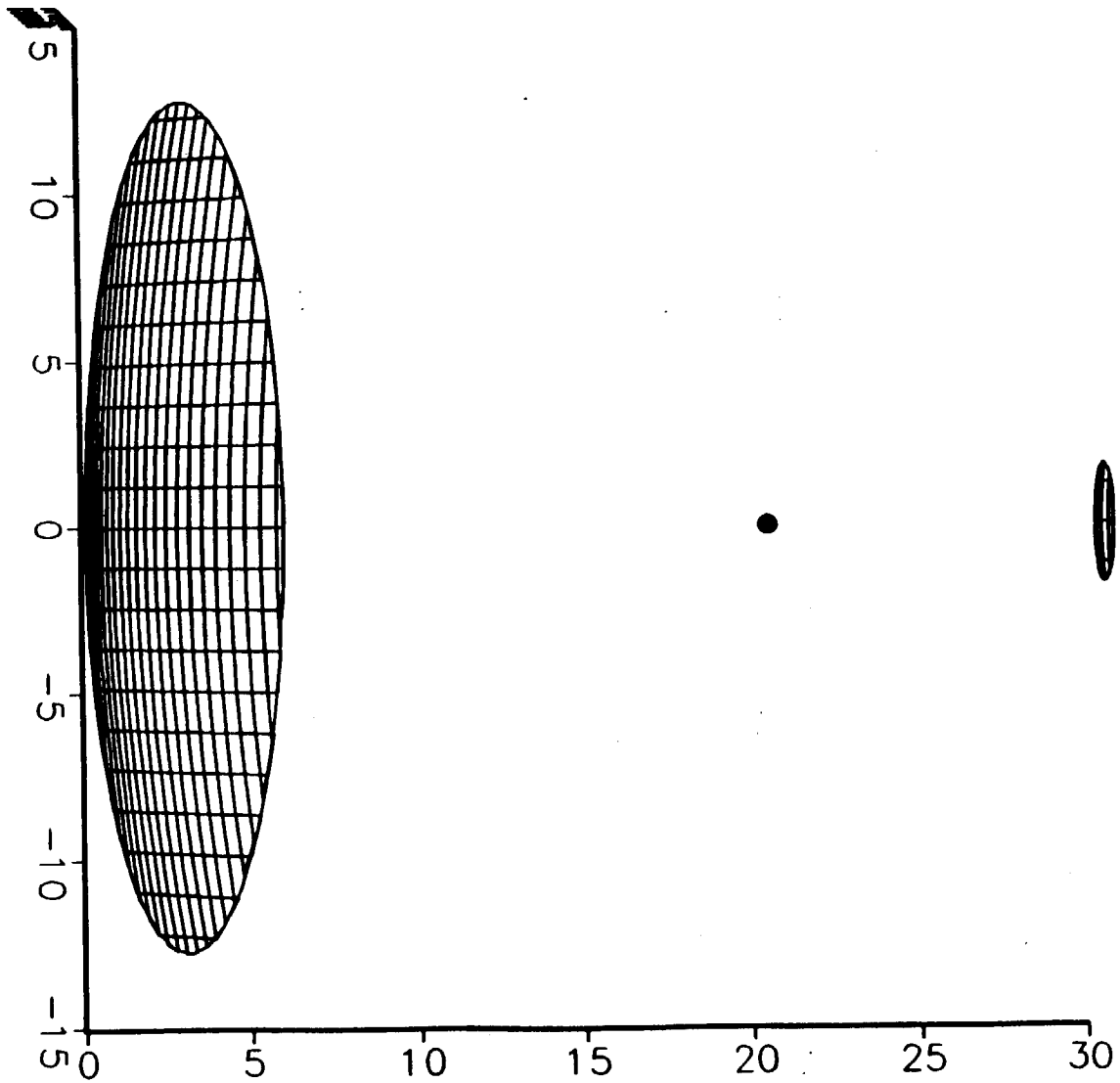

Figure 3.1-2 (b). Type 6 reflector antenna system (top view).

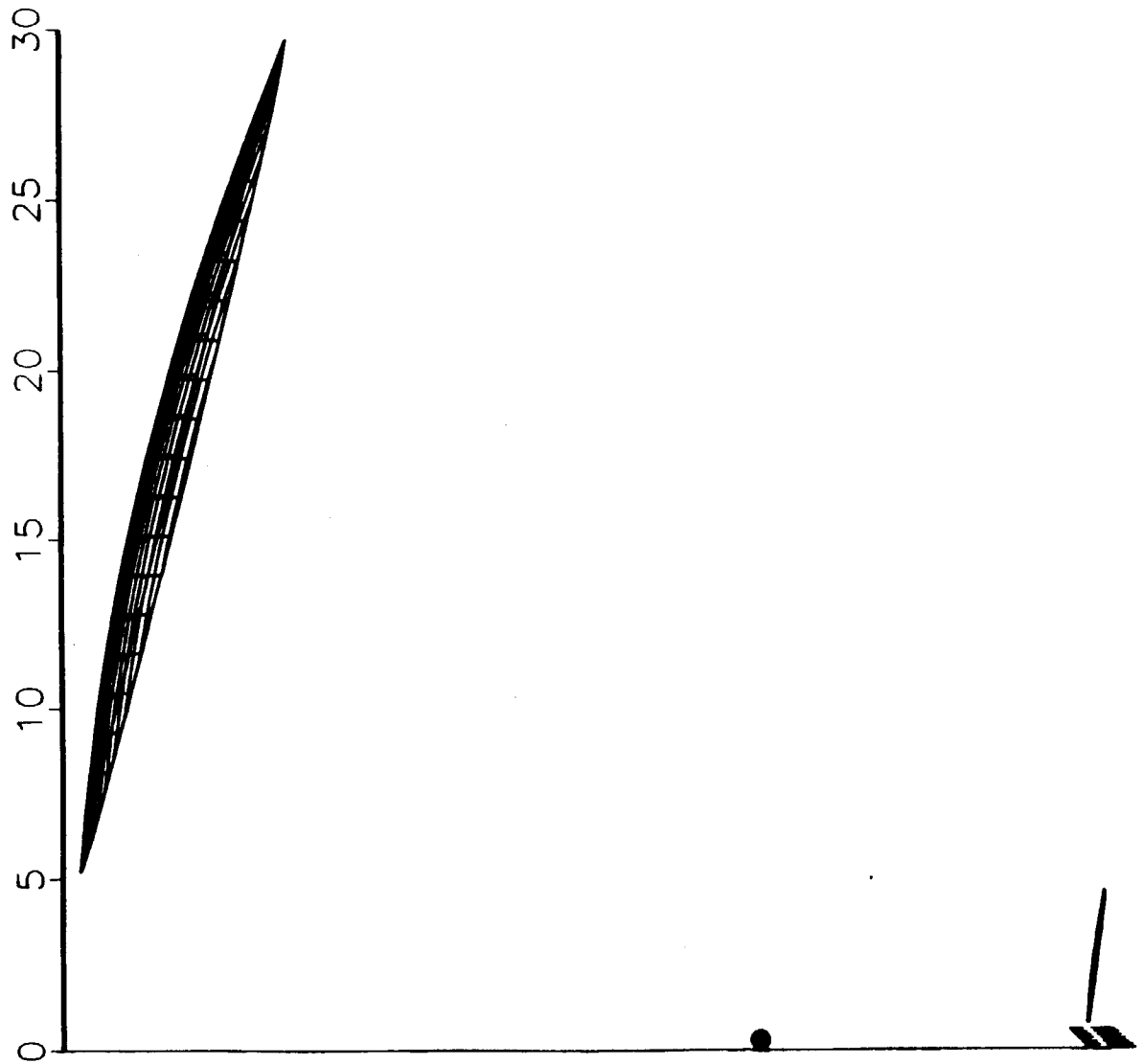

Figure 3.1-2 (c). Type 6 reflector antenna system (side view).

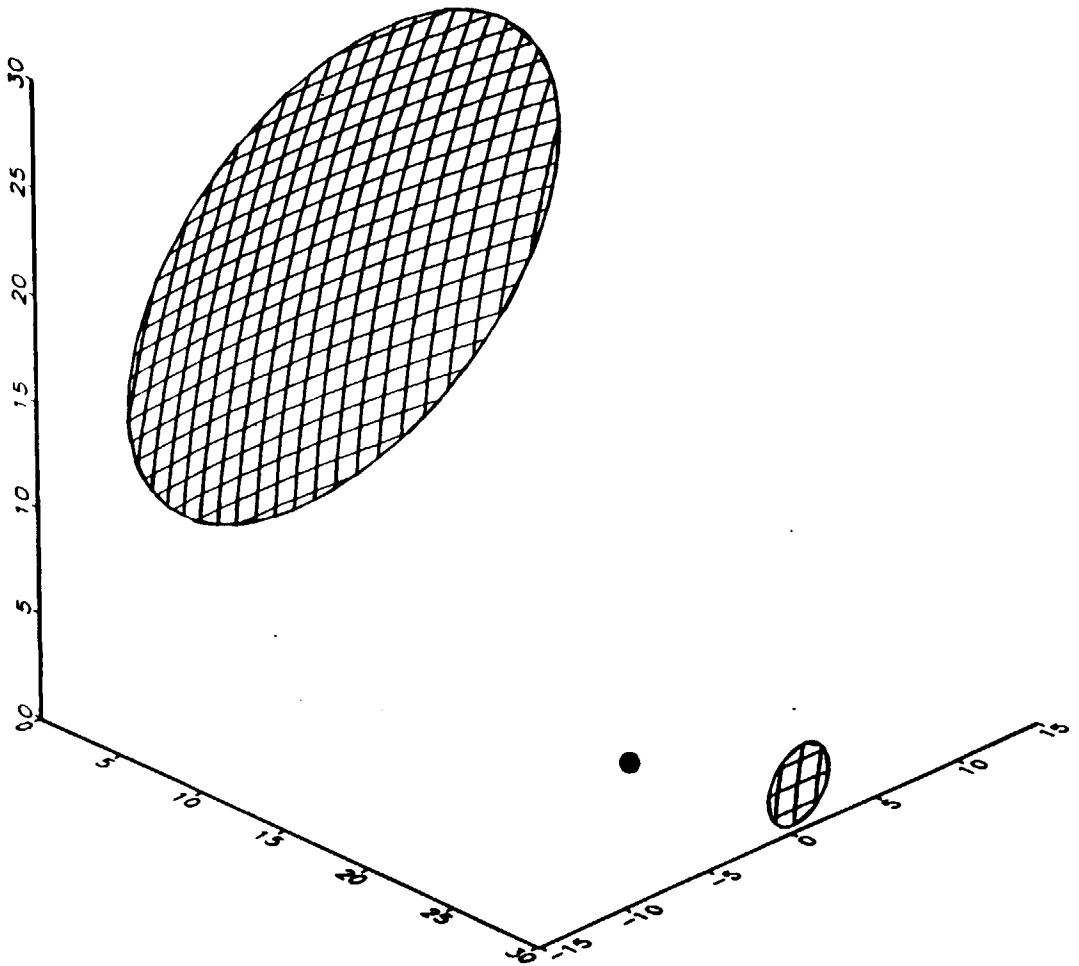

Figure 3.1-2 (d). Type 6 reflector antenna system.

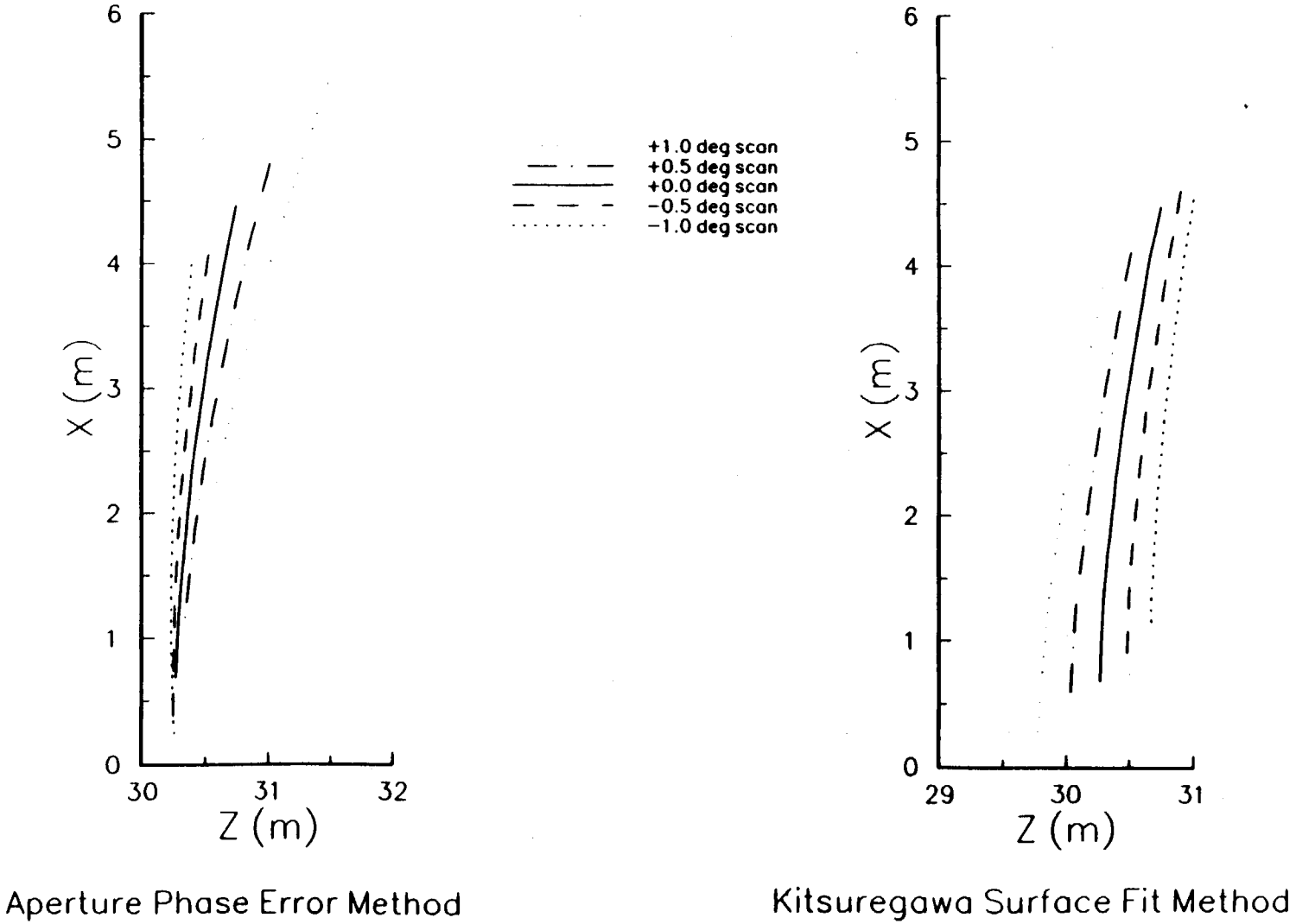

Figure 3.2-1. Type 6 reflector antenna system - scanned subreflector profiles.

GRASP7 input file is automatically written by DRAS-3D. This file includes the coefficients for an analytic definition of the subreflector by GRASP7. The equation used by GRASP7 to define the subreflector is

$$Ax^2 + Bxy + Cy^2 + Dx + Ey + F = Gz^2 + Hz + Ixz + Jyz \qquad (3\text{-}2)$$

The coefficients are found from the translated focal points of the unscanned subreflector. This improvement allows the use of a GTD-PO electromagnetic analysis of the system by GRASP7 which reduces the analysis time by a factor of approximately 15. Also, by limiting the extent of the far-field patterns cuts to constant number of beamwidths, the analysis time is essentially frequency independent.

3.3 Electromagnetic Analysis Results - Nominal Case

The Type 6 reflector antenna system electromagnetics analyses are performed using the TICRA GRASP7 analysis package. The original nominal case consists of a 25-meter main reflector, a 4.5-meter subreflector, and a Gaussian beam feed which provides an edge taper of ~ 15 dB. At 10 GHz, the unscanned system produces a main beam gain of ~ 67 dB, a first sidelobe level of ~ 28, and a half-power beamwidth of $\sim 0.08^{\circ}$. The system is capable of scanning over approximately a 1.0° range with a 1 dB scan loss. The most severe limitation on scan performance occurs in the $\phi = 0^{\circ}$ direction and seems to be largely illumination induced. Figure 3.3-1 shows the spillover loss for the scanned 25 meter system. The main beam peak gain for the antenna system is shown in Fig. 3.3-2 (a-c) at 10, 20, and 40 GHz. First sidelobe levels are shown for the Type 6 antenna system as a function of scan angle in Fig. 3.3-3 (a-c). The combination of high spillover in the direction of highest scan loss ($\phi = 0^{\circ}$) combined with the comparable scan loss and sidelobe levels at the three frequencies seems to indicate that the error function could be further improved through the inclusion of a illumination term. Sample patterns for the 25 meter system unscanned and scanned to 0.5° from boresight in each of the 45° planes are shown in Fig. 3.3-4 (a-f). These pattern plots each contain four cuts separated by 45° in ϕ angle.

3.4 Three Dimensional Mizugutch Condition - Electromagnetics Analysis Results

The analysis of the Type 6 reflector antenna system satisfying the Mizugutch condition was performed by GTD-PO using the GRASP7 package. The reflector system was synthesized to fulfill the Mizugutch minimum cross-polarization condition and create an axi-symmetric equivalent paraboloid as developed by Ko Takamizawa. The analysis was performed for a system using the NASA Langley Type 6 test article with a 1.5 meter subreflector. A frequency of 23.36 GHz was chosen because it yields an electrical size of the antenna to the electrical size of the 25 meter system at 10 GHz. This allows direct comparison of the results shown in the previous section with the analysis results for this

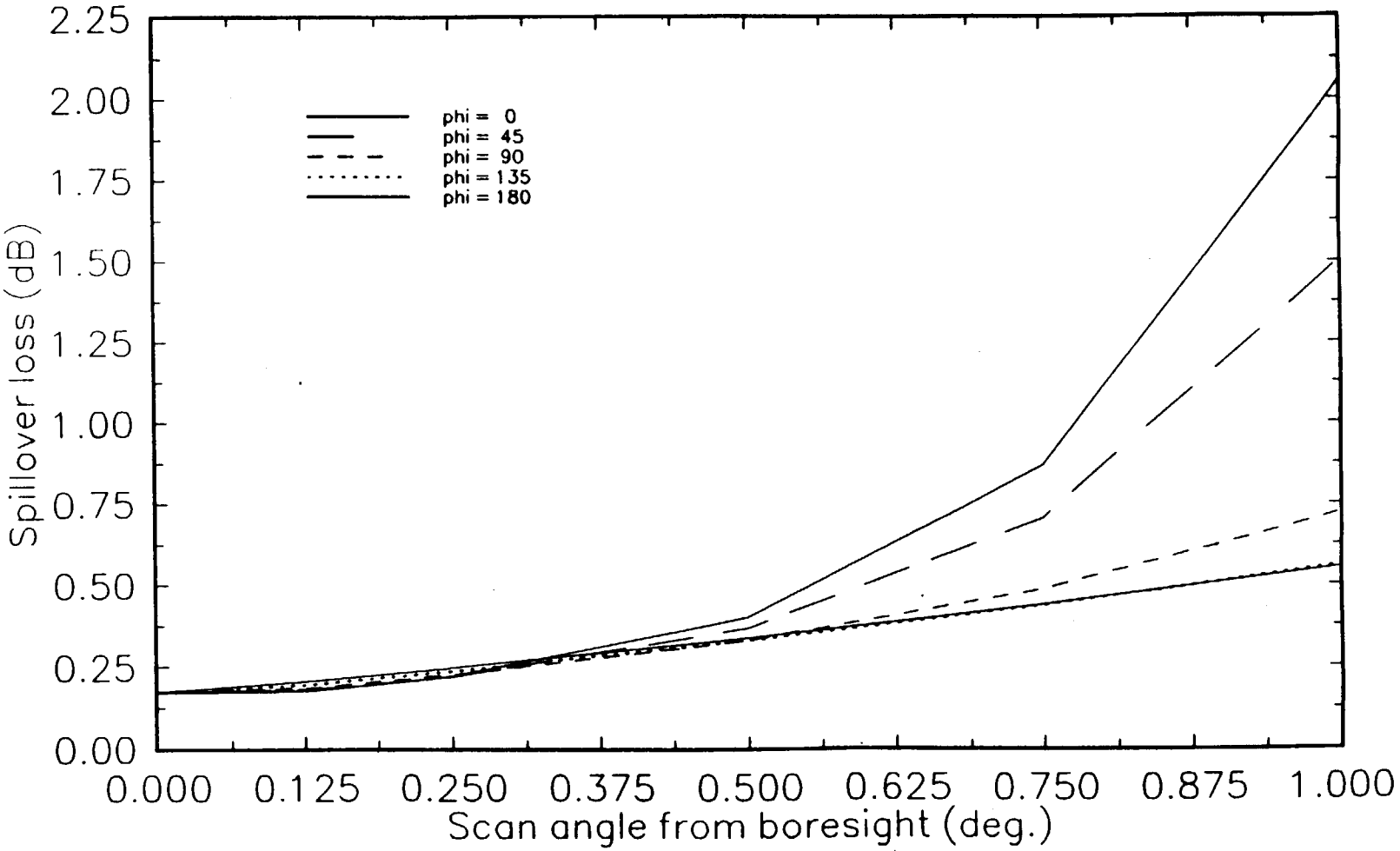

Figure 3.3-1. Type 6 reflector antenna system - 25 m, spillover loss.

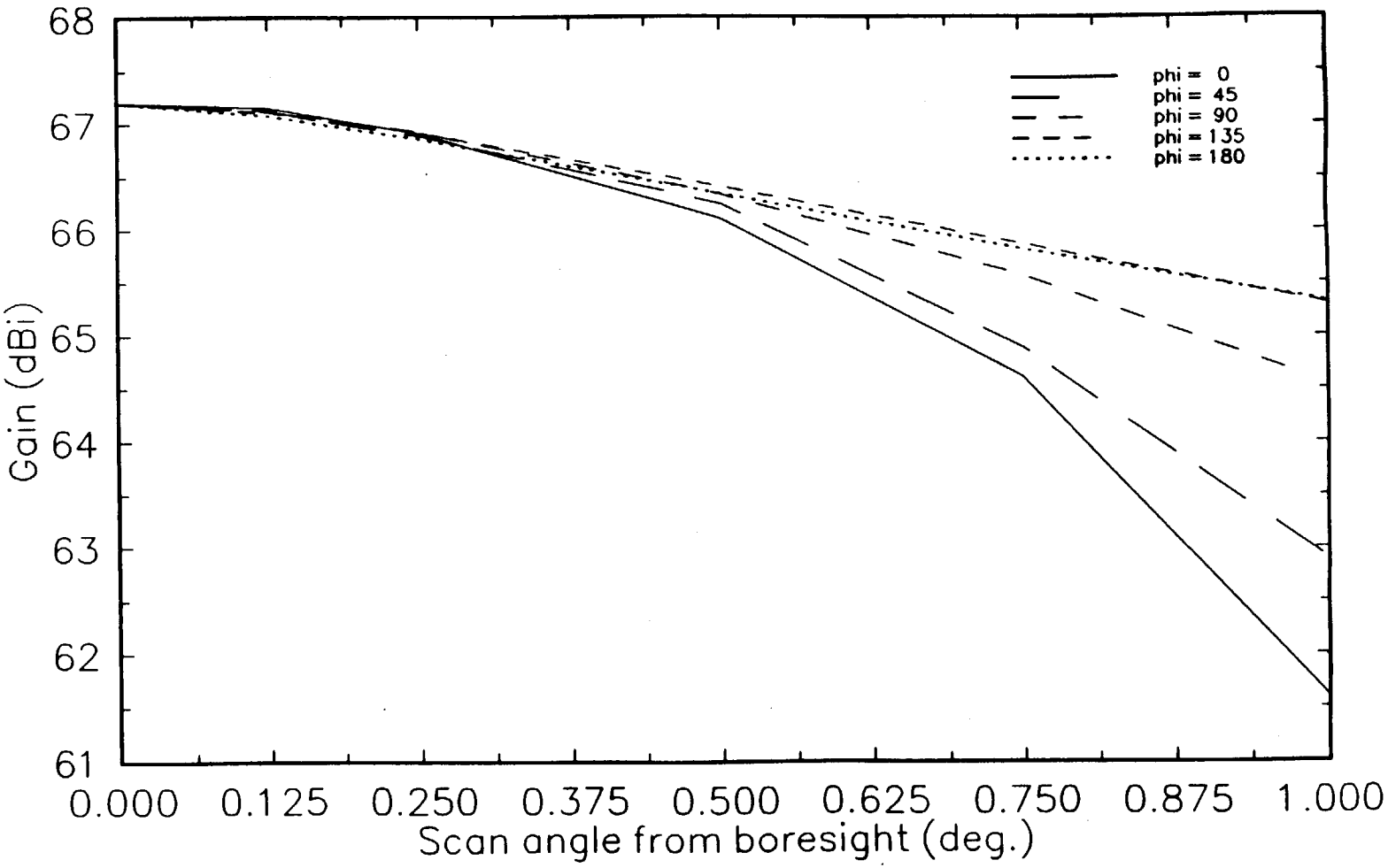

Figure 3.3-2 (a). Type 6 reflector antenna system - 25 m, 10 GHz main beam gain.

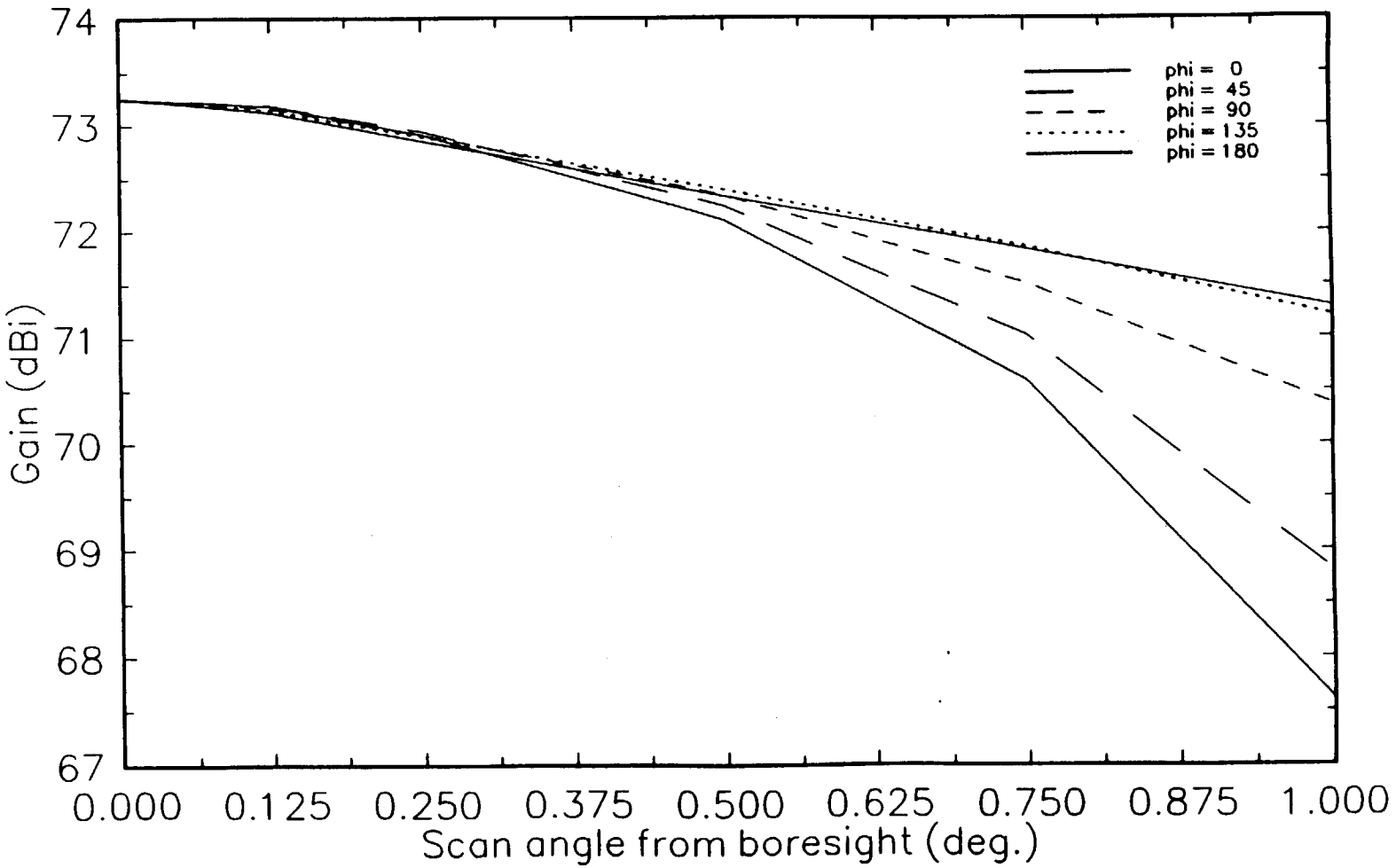

Figure 3.3-2 (b). Type 6 reflector antenna system - 25 m, 20 GHz main beam gain.

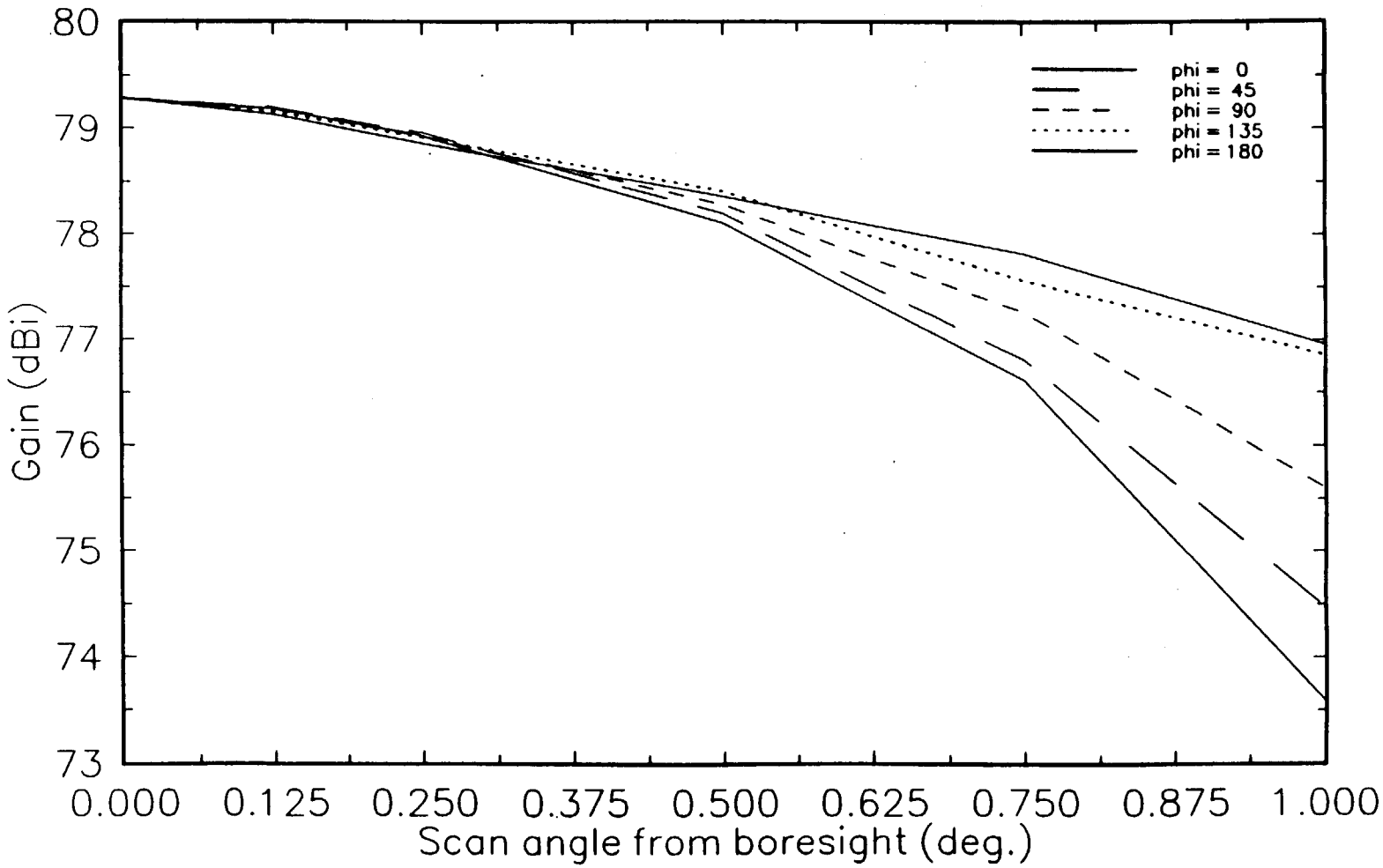

Figure 3.3-2 (c). Type 6 reflector antenna system - 25 m, 40 GHz main beam gain.

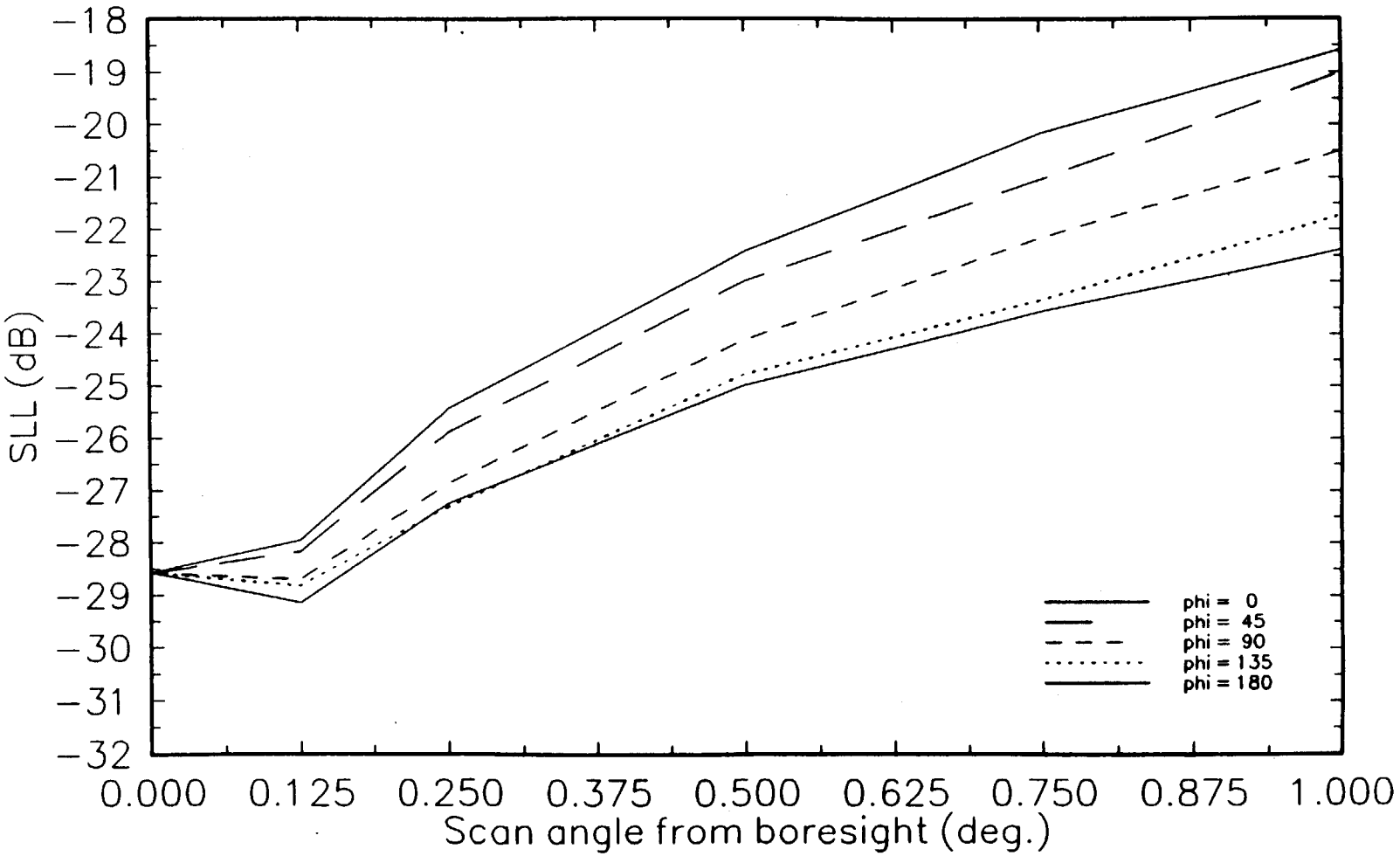

Figure 3.3-3 (a). Type 6 reflector antenna system - 25 m, 10 GHz sidelobe level.

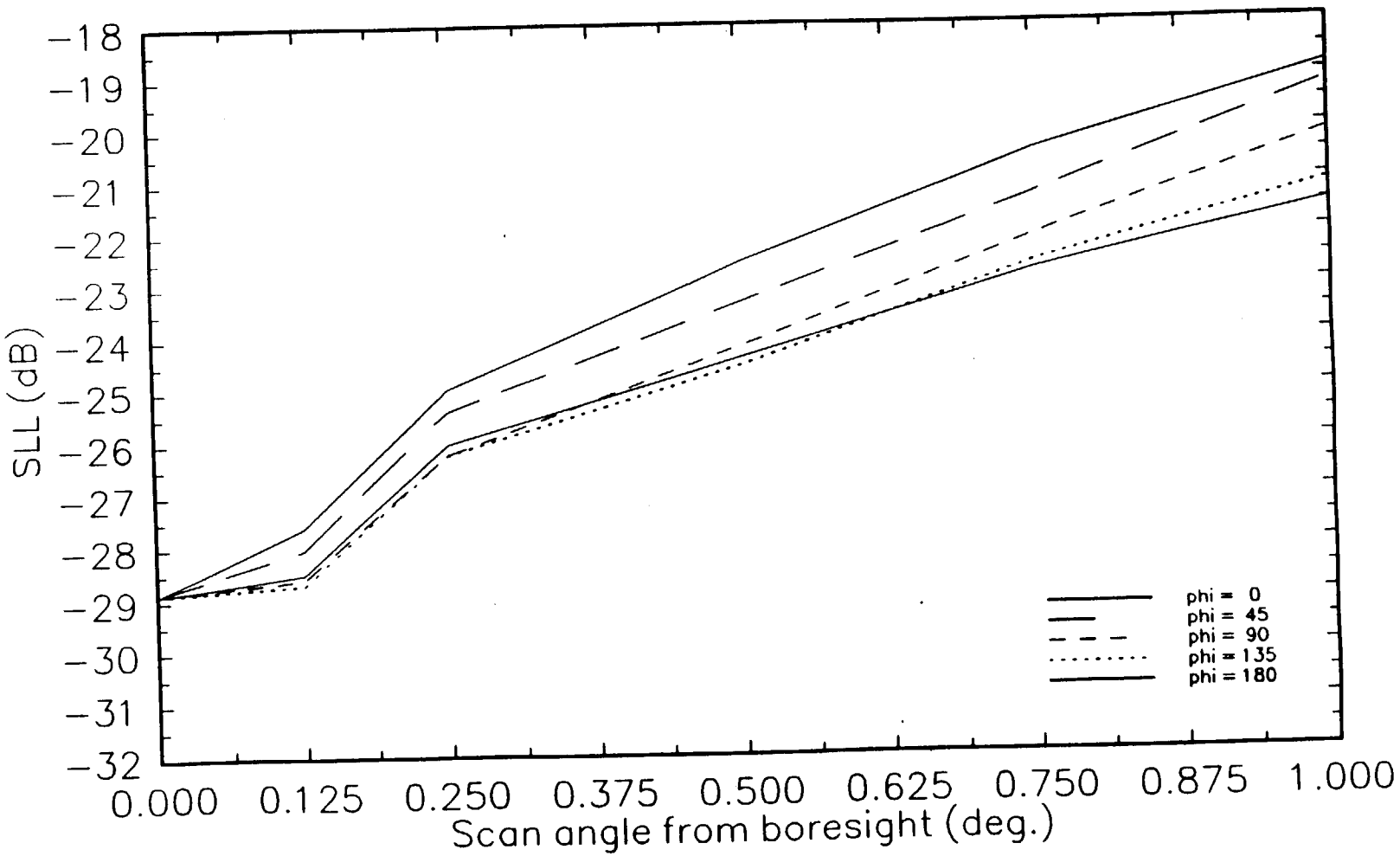

Figure 3.3-3 (b). Type 6 reflector antenna system - 25 m, 20 GHz sidelobe level.

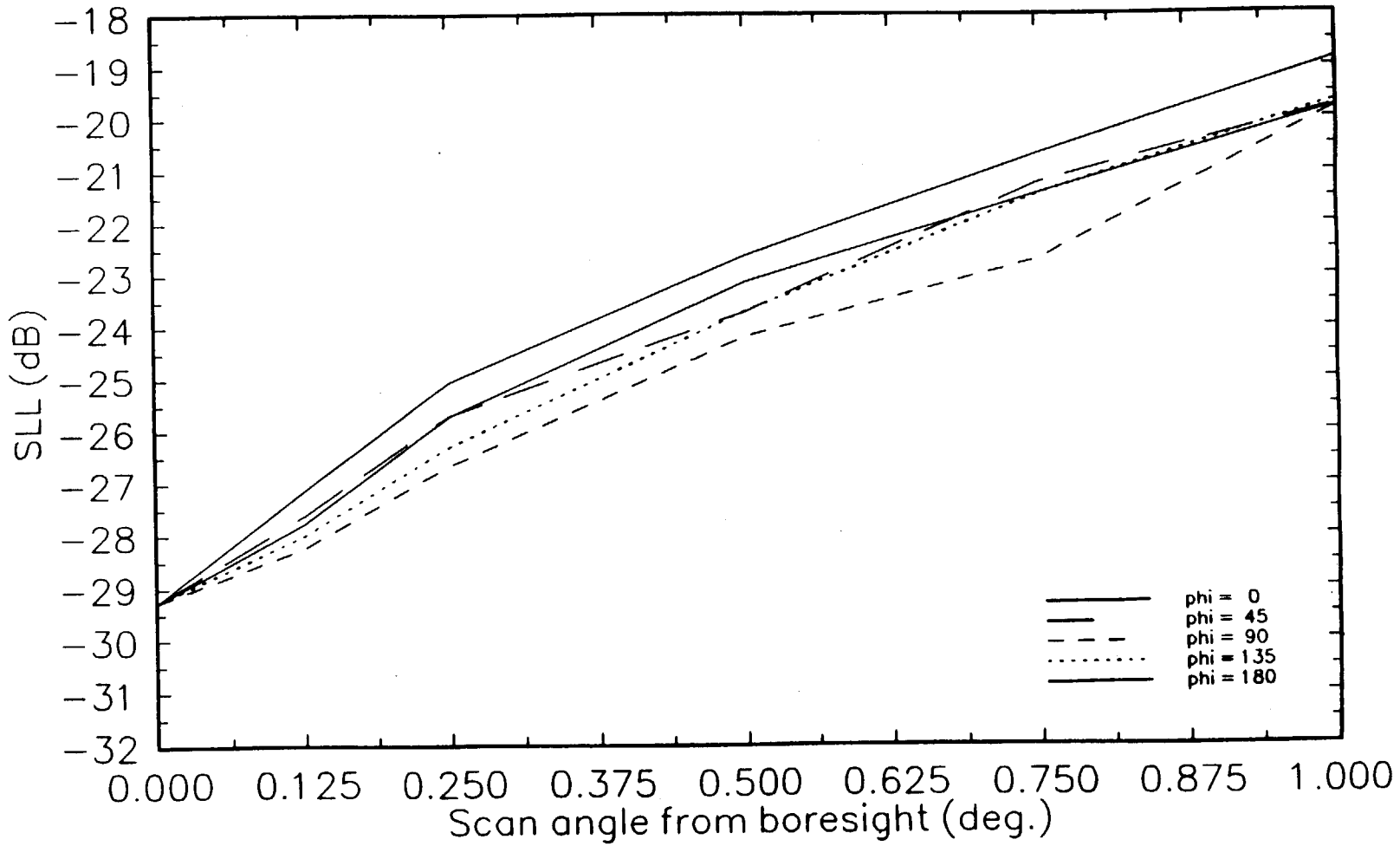

Figure 3.3-3 (c). Type 6 reflector antenna system - 25 m, 40 GHz sidelobe level.

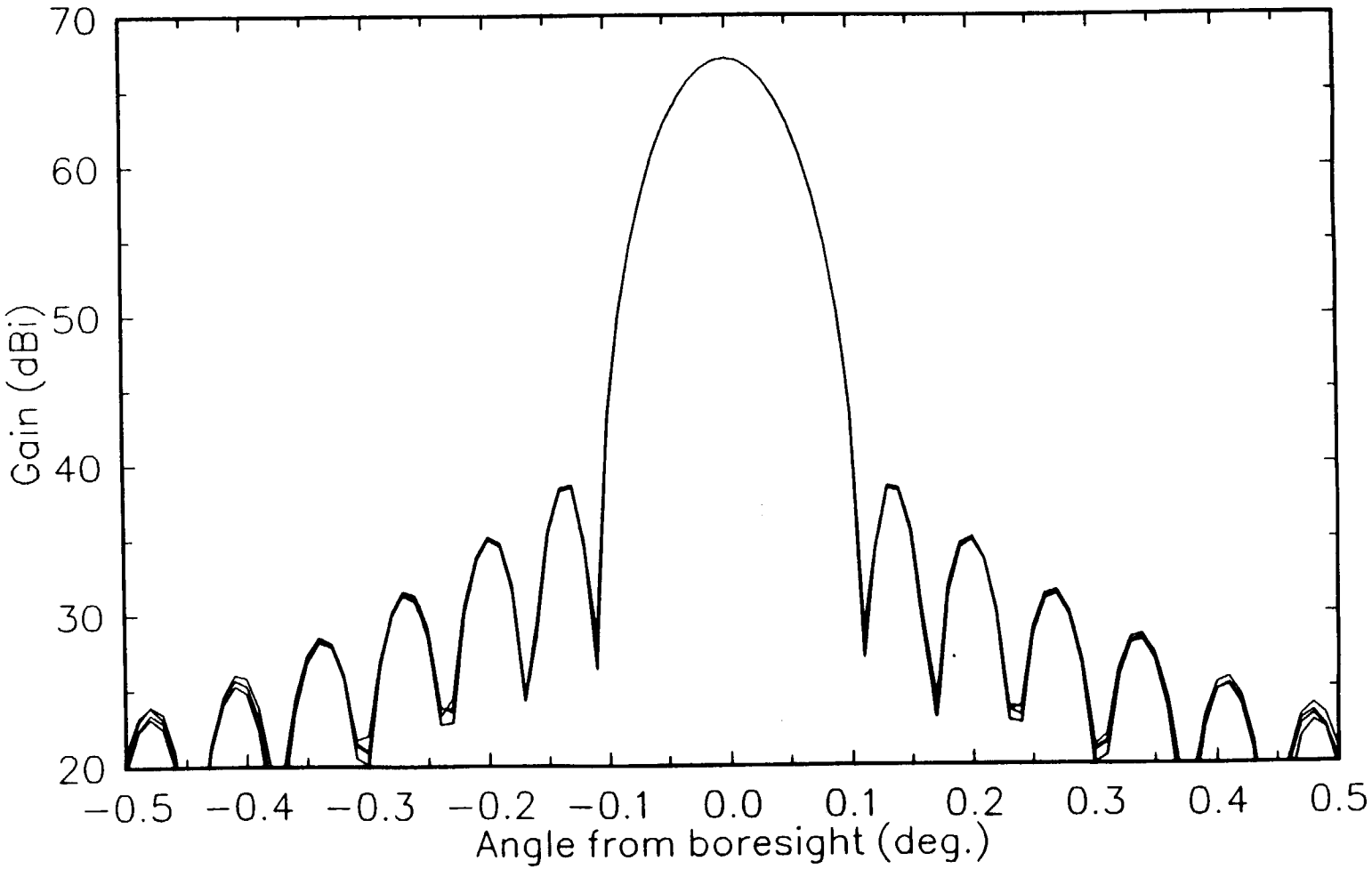

Figure 3.3-4 (a). Type 6 reflector antenna system - 25 m, 10 GHz, $\phi = 0^{\circ}$, $\theta = 0.0^{\circ}$.

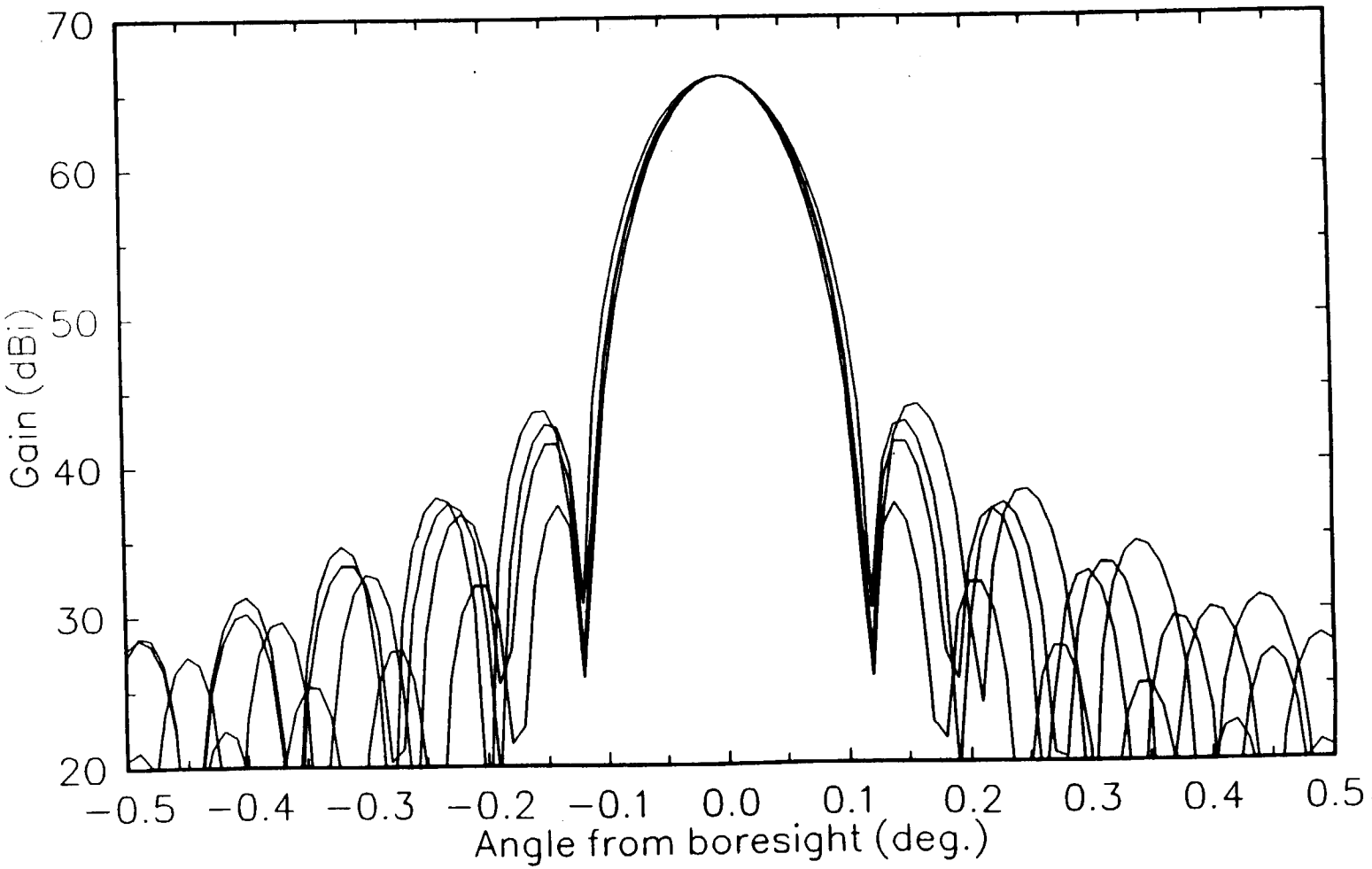

Figure 3.3-4 (b). Type 6 reflector antenna system - 25 m, 10 GHz, $\varphi = 0^{\circ}$, $\theta = 0.5^{\circ}$.

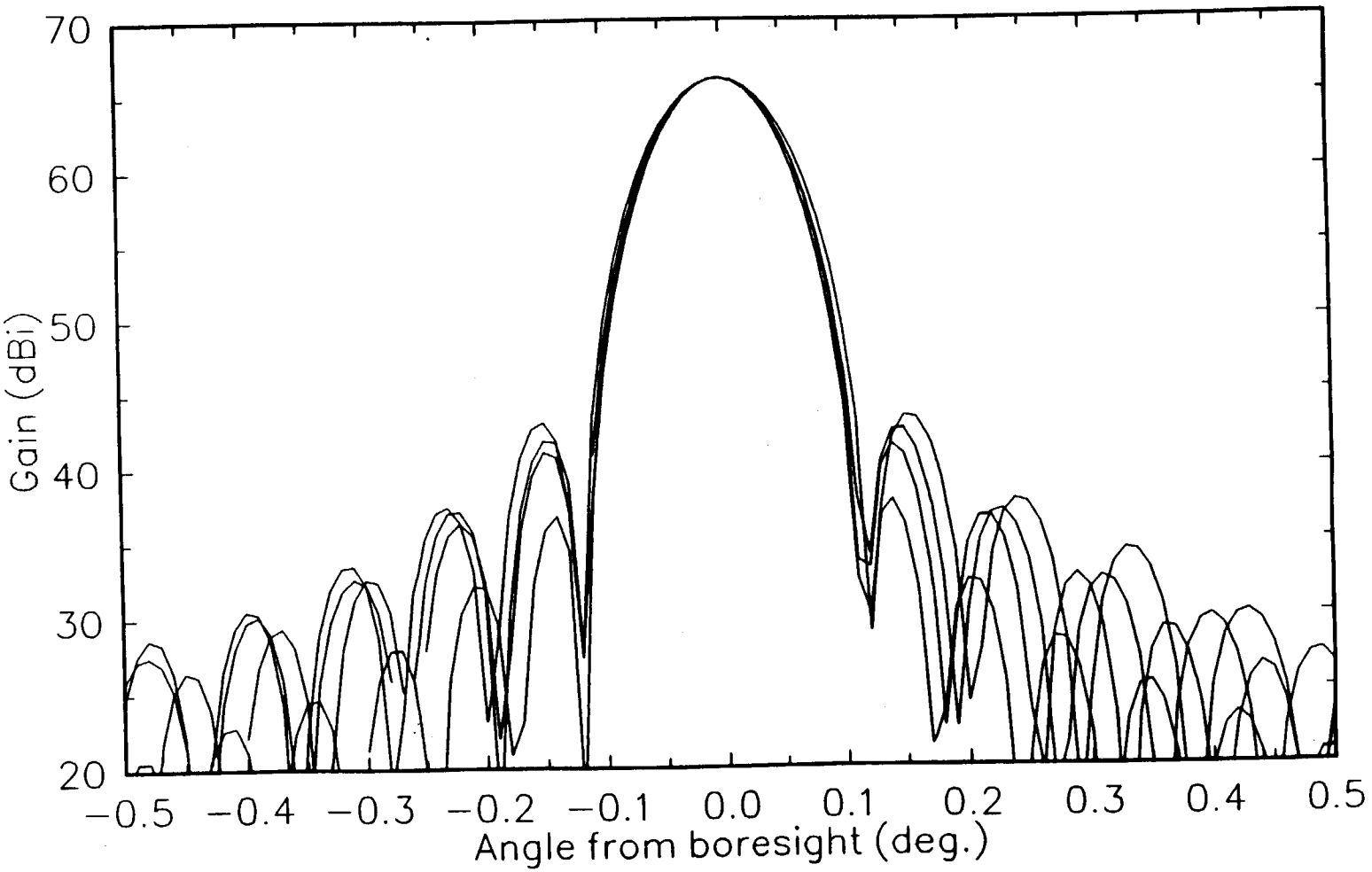

Figure 3.3-4 (c). Type 6 reflector antenna system - 25 m, 10 GHz, $\phi = 45°$, $\theta = 0.5°$.

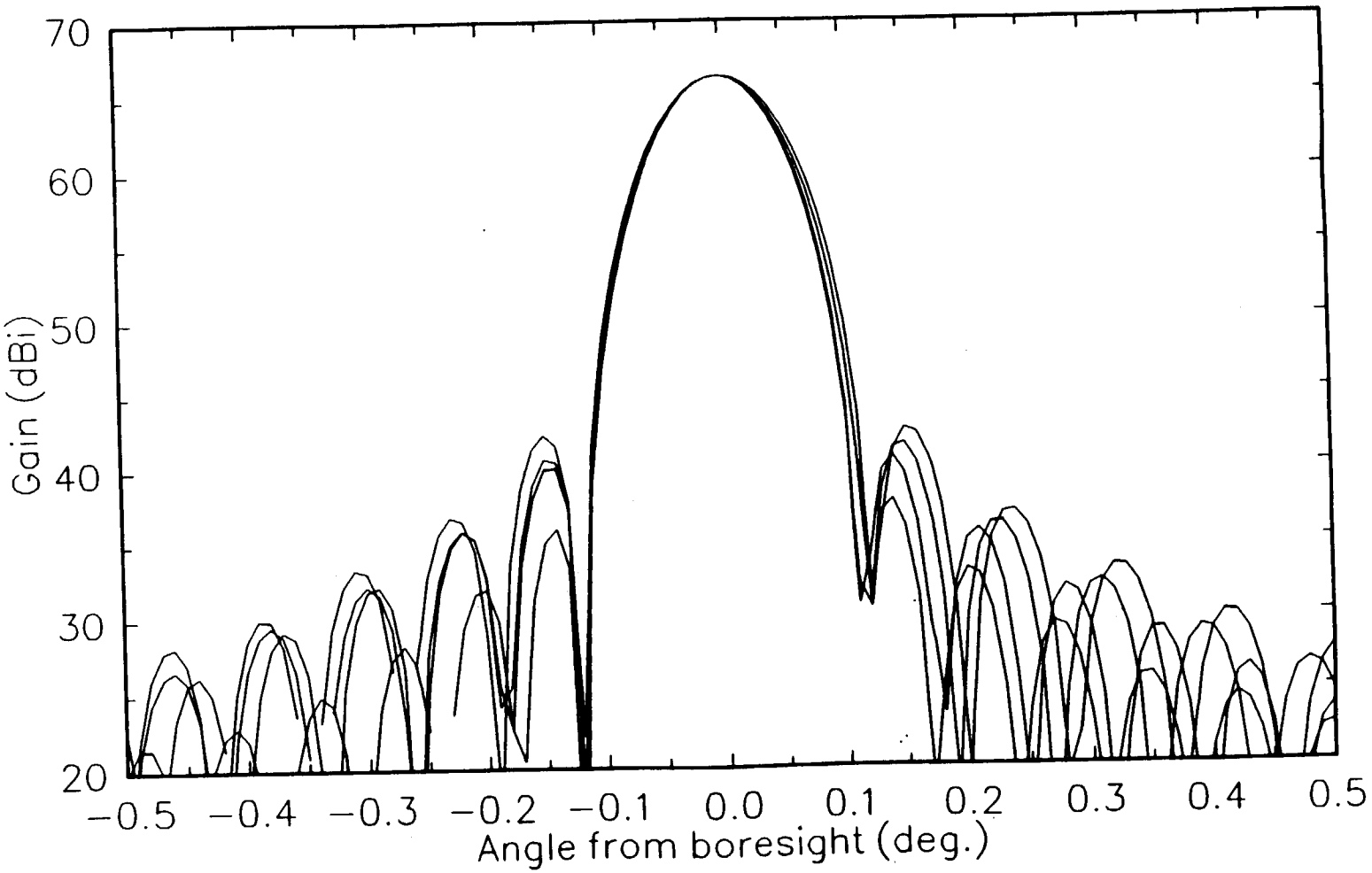

Figure 3.3-4 (d). Type 6 reflector antenna system - 25 m, 10 GHz, $\phi = 90^{\circ}$, $\theta = 0.5^{\circ}$.

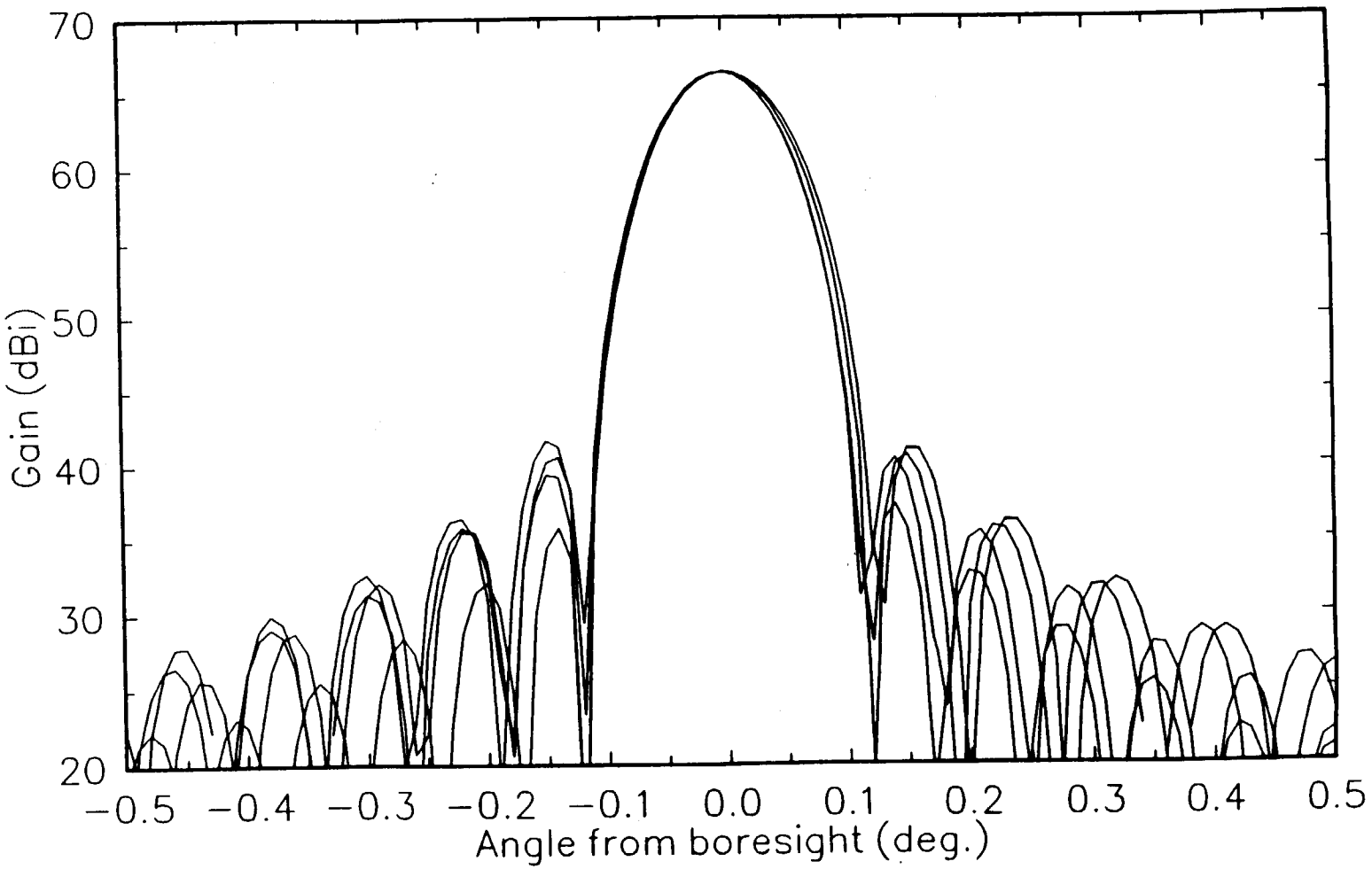

Figure 3.3-4 (e). Type 6 reflector antenna system - 25 m, 10 GHz, $\phi = 135$, $\theta = 0.5^{\circ}$.

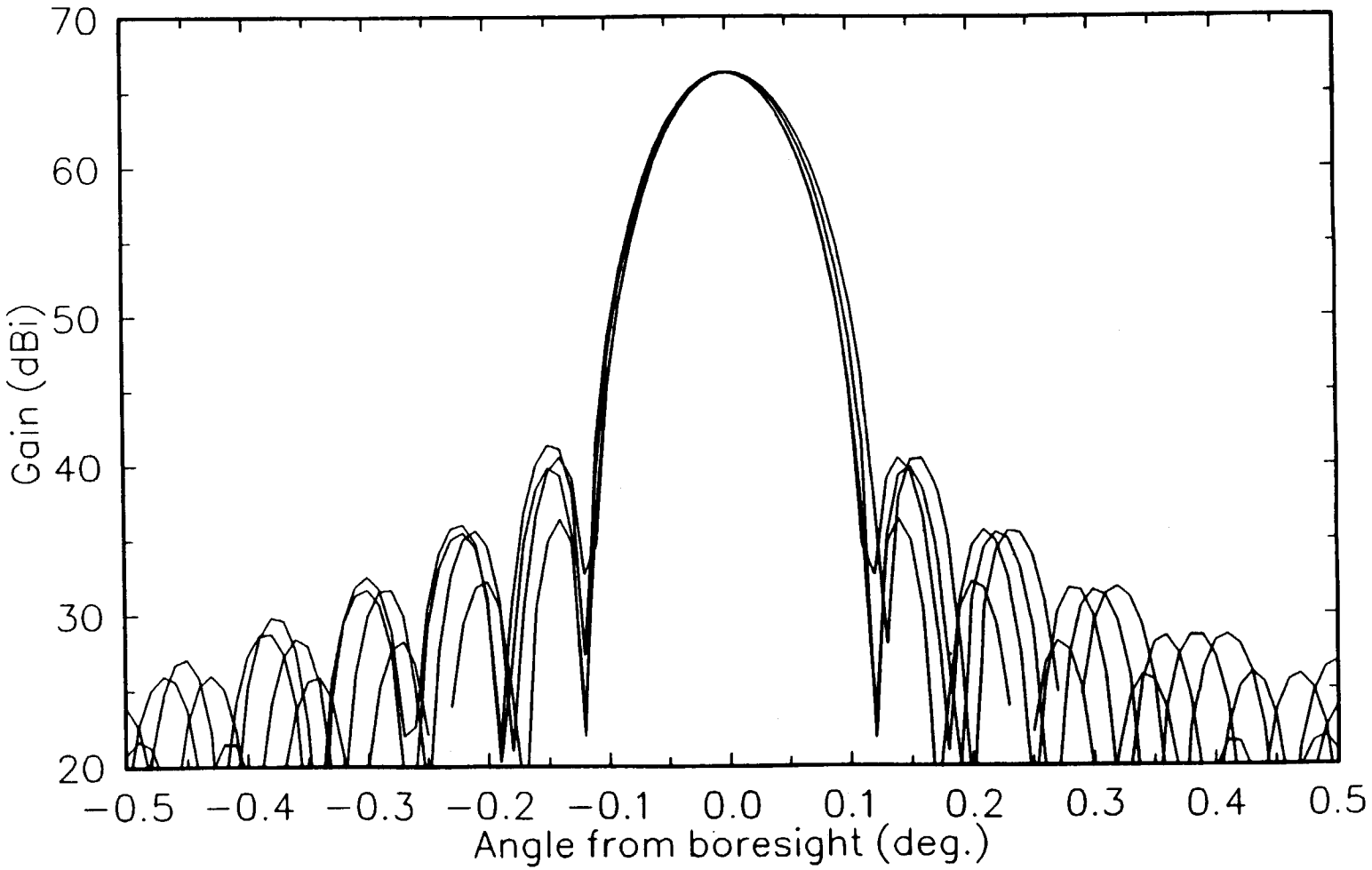

Figure 3.3-4 (f). Type 6 reflector antenna system - 25 m, 10 GHz, $\phi = 180^{\circ}$, $\theta = 0.5^{\circ}$.

system. The spillover loss of the system is shown in Fig. 3.4-1. Although the loss for scan in the $\phi = 0$ plane is still higher than for other planes, the maximum loss is reduced by about 0.6 dB. Peak main beam gain for the scanned system, shown in Fig. 3.4-2, exhibits a scan loss which is about 1.7 dB lower than for the 25 meter case shown in Fig. 3.3-2 (a). First sidelobe levels shown in Fig. 3.4-3 are comparable for the two systems. Figure 3.3-3 (a-f) shows the far-field patterns of the Mizugutch condition system scanned 0.5° from boresight in each of the 45 planes.

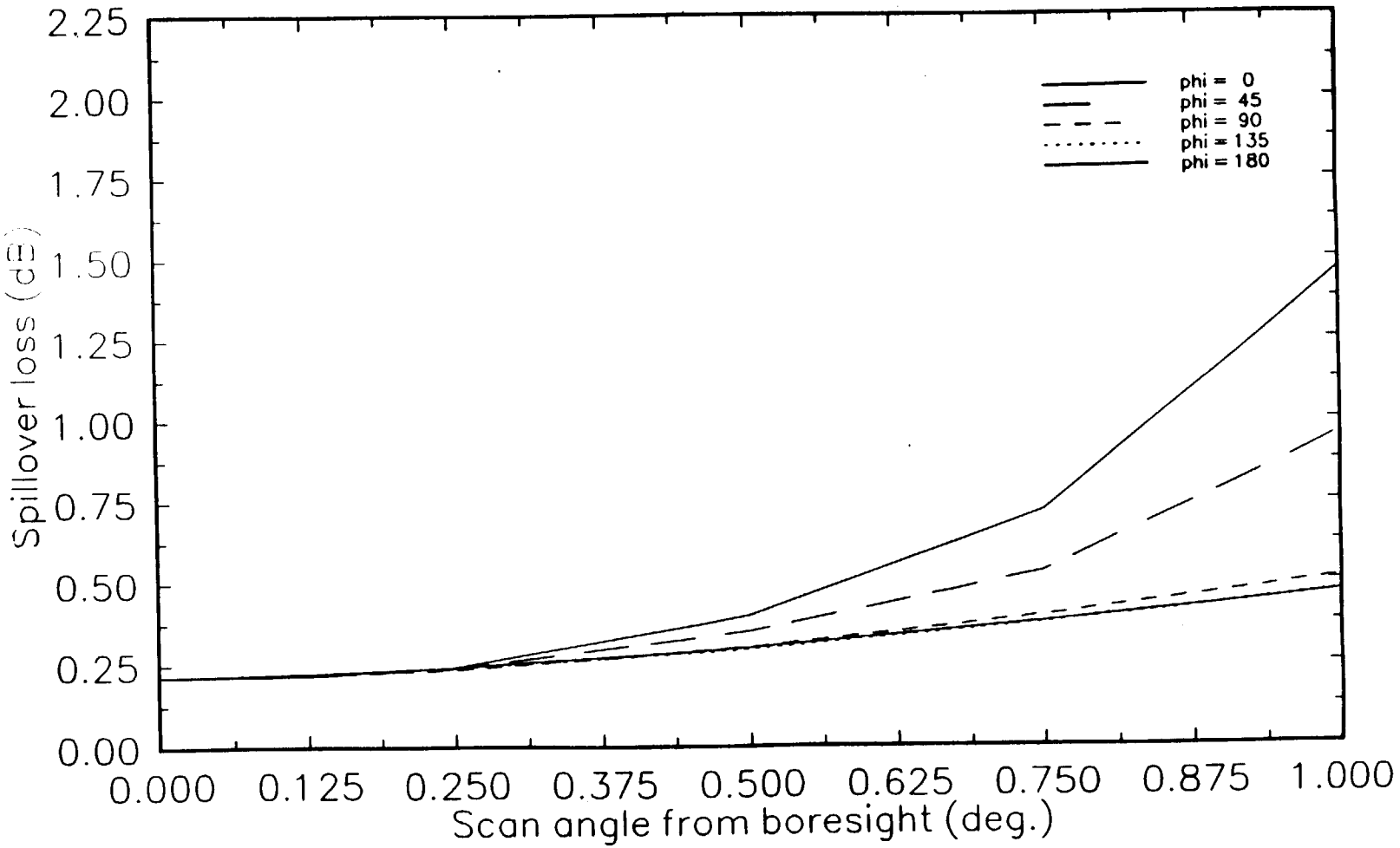

Figure 3.4-1. Type 6 reflector antenna system - 10.7 m, spillover loss.

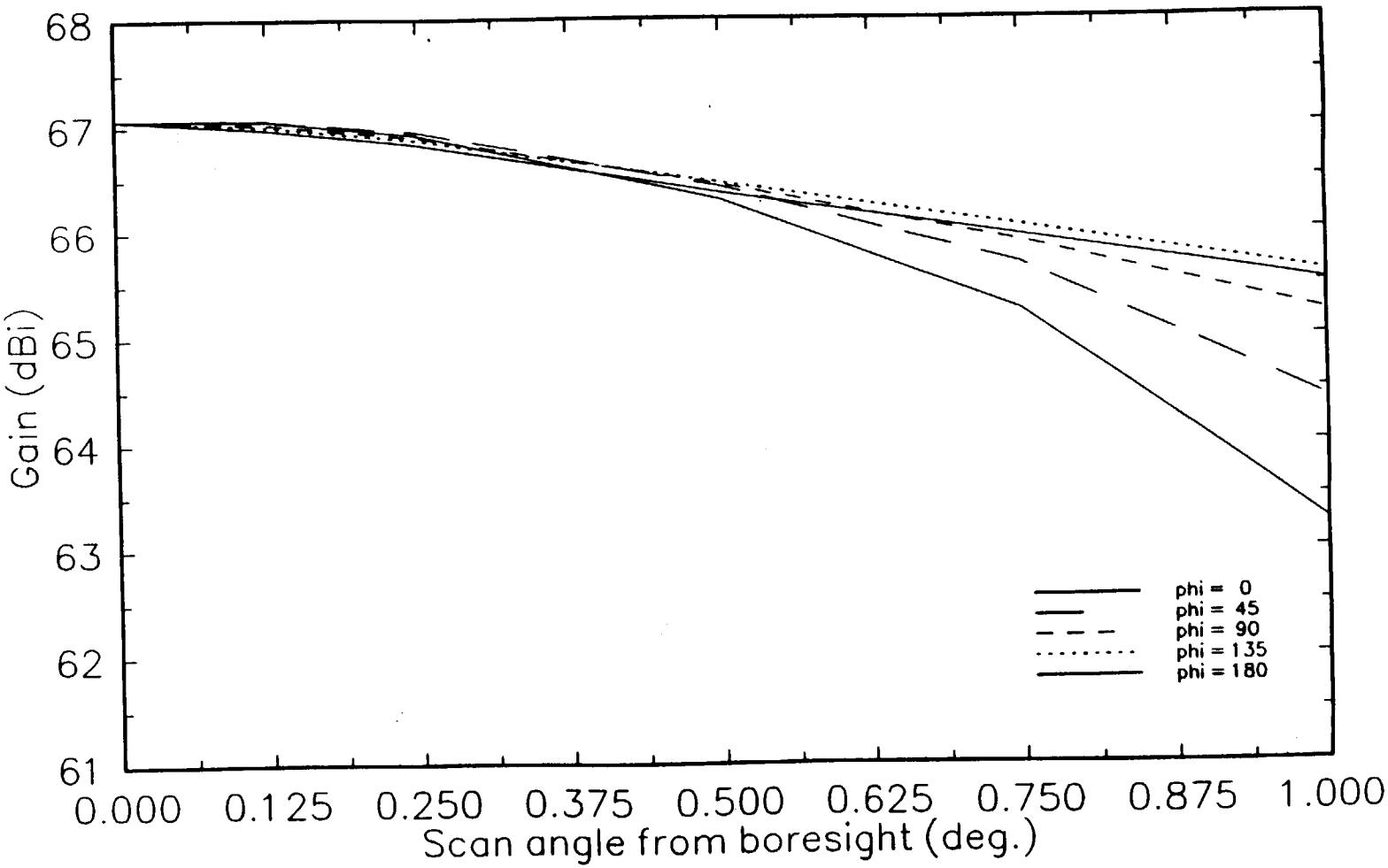

Figure 3.4-2. Type 6 reflector antenna system - 10.7 m, 23.36 GHz main beam gain.

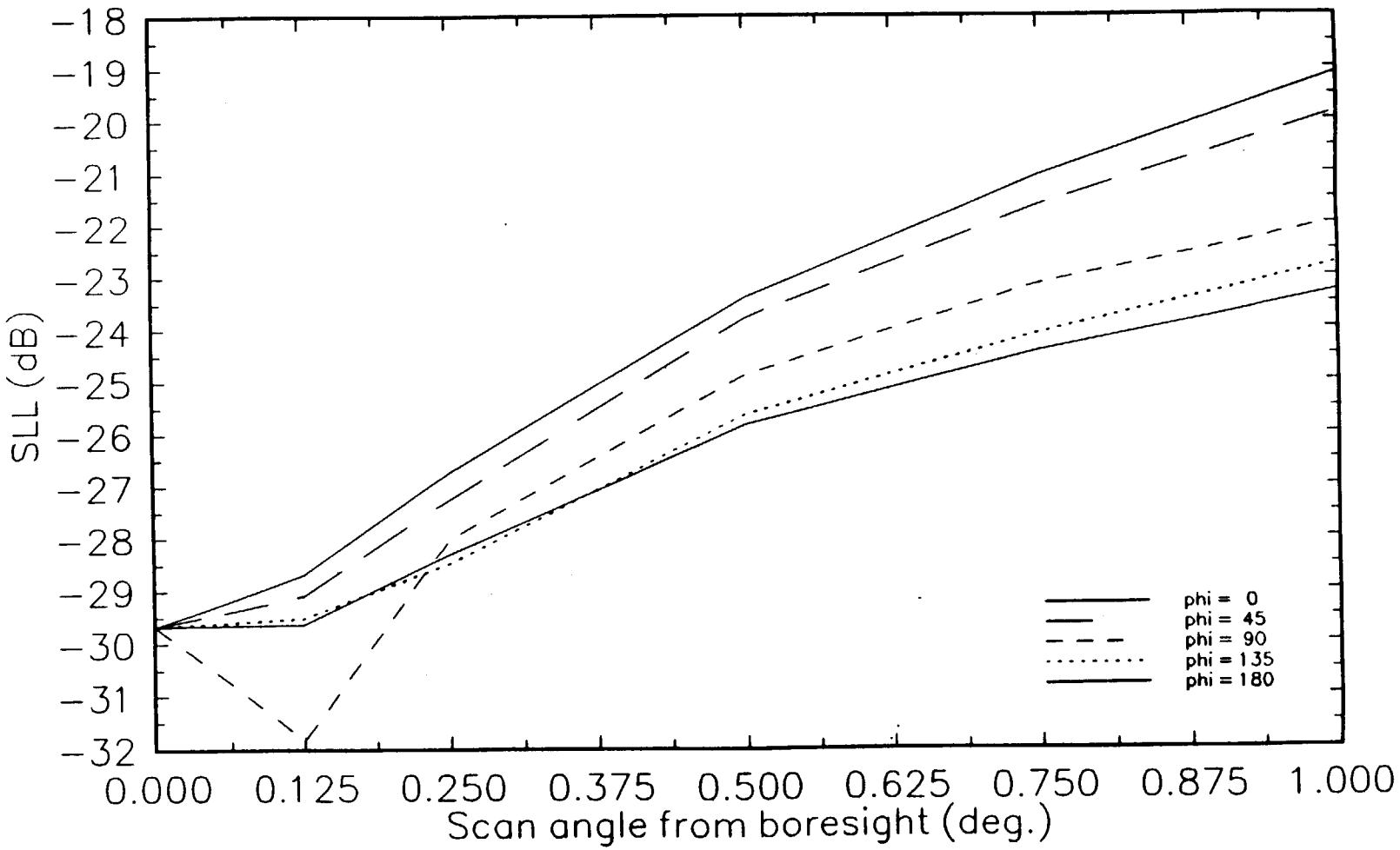

Figure 3.4-3. Type 6 reflector antenna system - 10.7 m, 23.36 GHz sidelobe level.

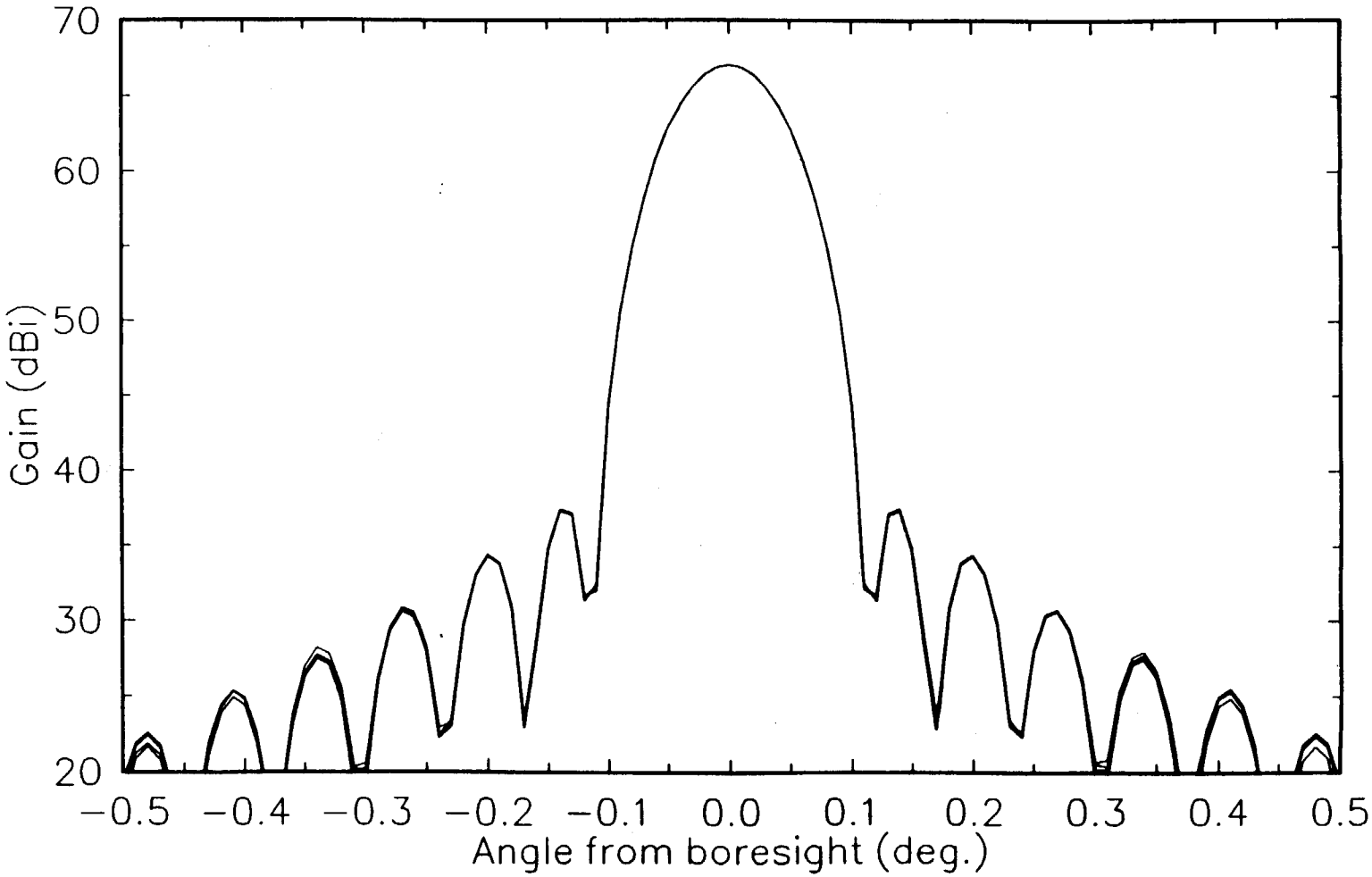

Figure 3.4-4 (a). Type 6 reflector antenna system - 10.7 m, 23.36 GHz, $\phi = 0^{\circ}$, $\theta = 0.0^{\circ}$.

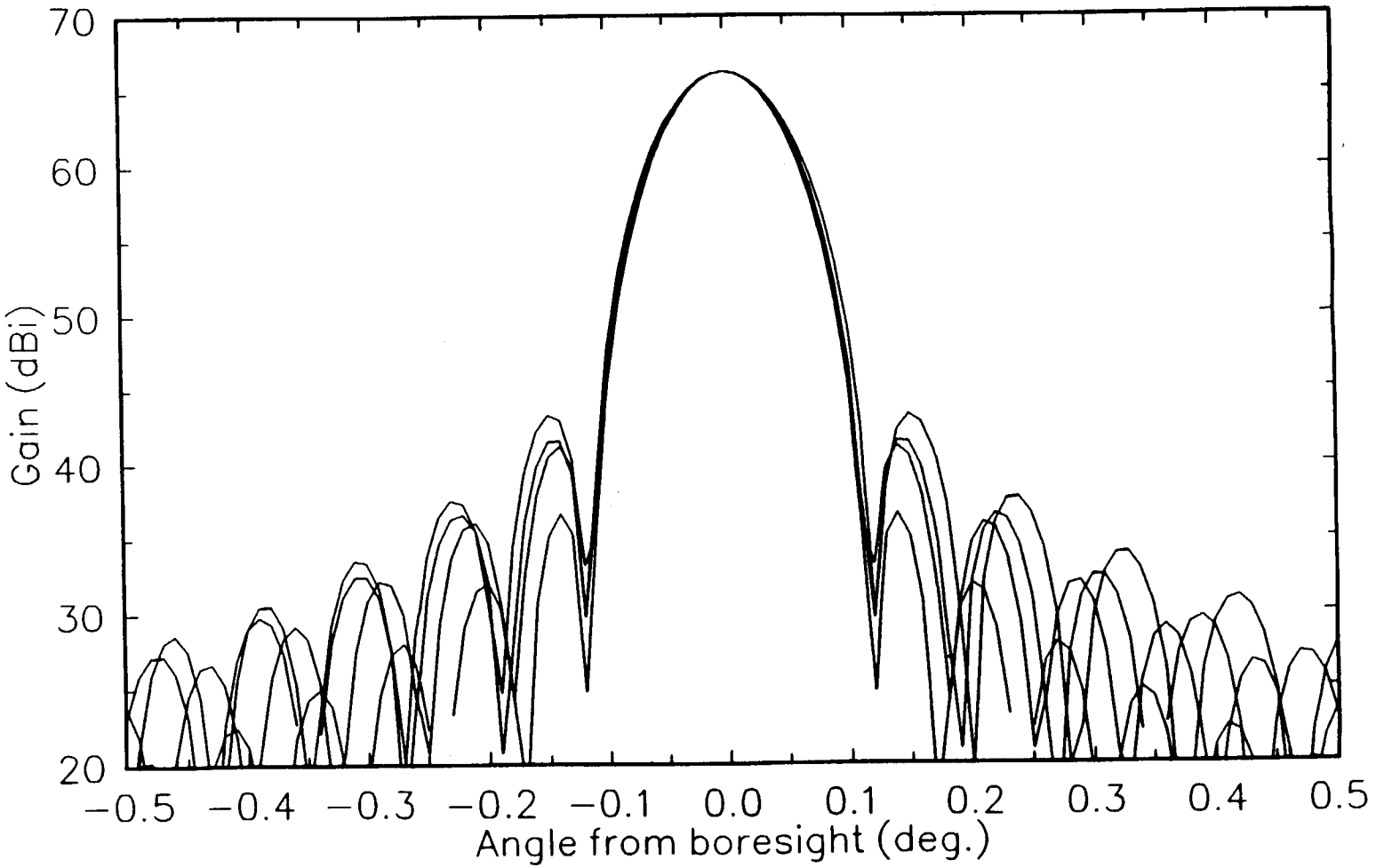

Figure 3.4-4 (b). Type 6 reflector antenna system - 10.7 m, 23.36 GHz, $\phi = 0^{\circ}$, $\theta = 0.5^{\circ}$.

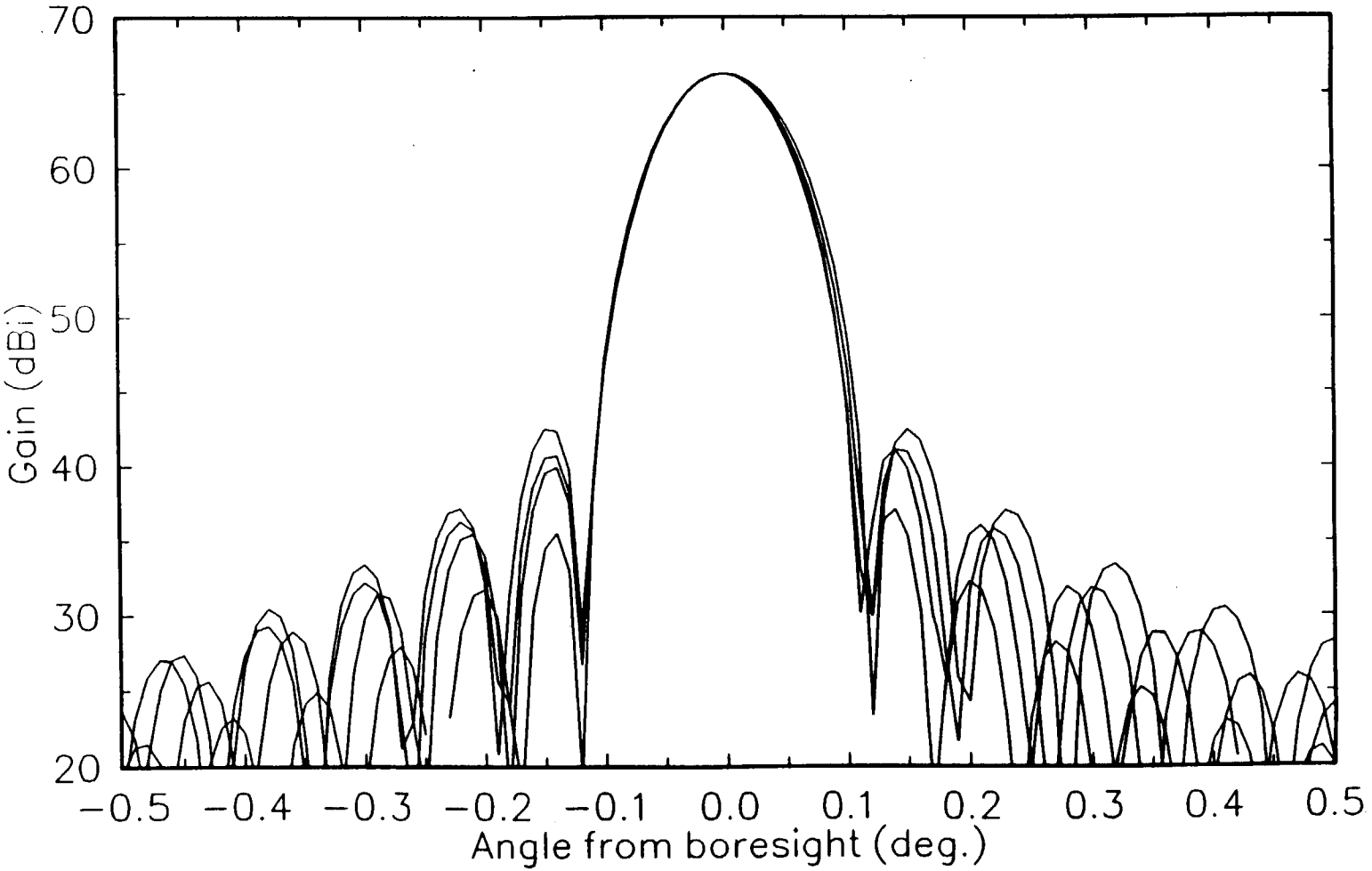

Figure 3.3-4 (c). Type 6 reflector antenna system - 10.7 m, 23.36 GHz, $\phi = 45^{\circ}$, $\theta = 0.5^{\circ}$.

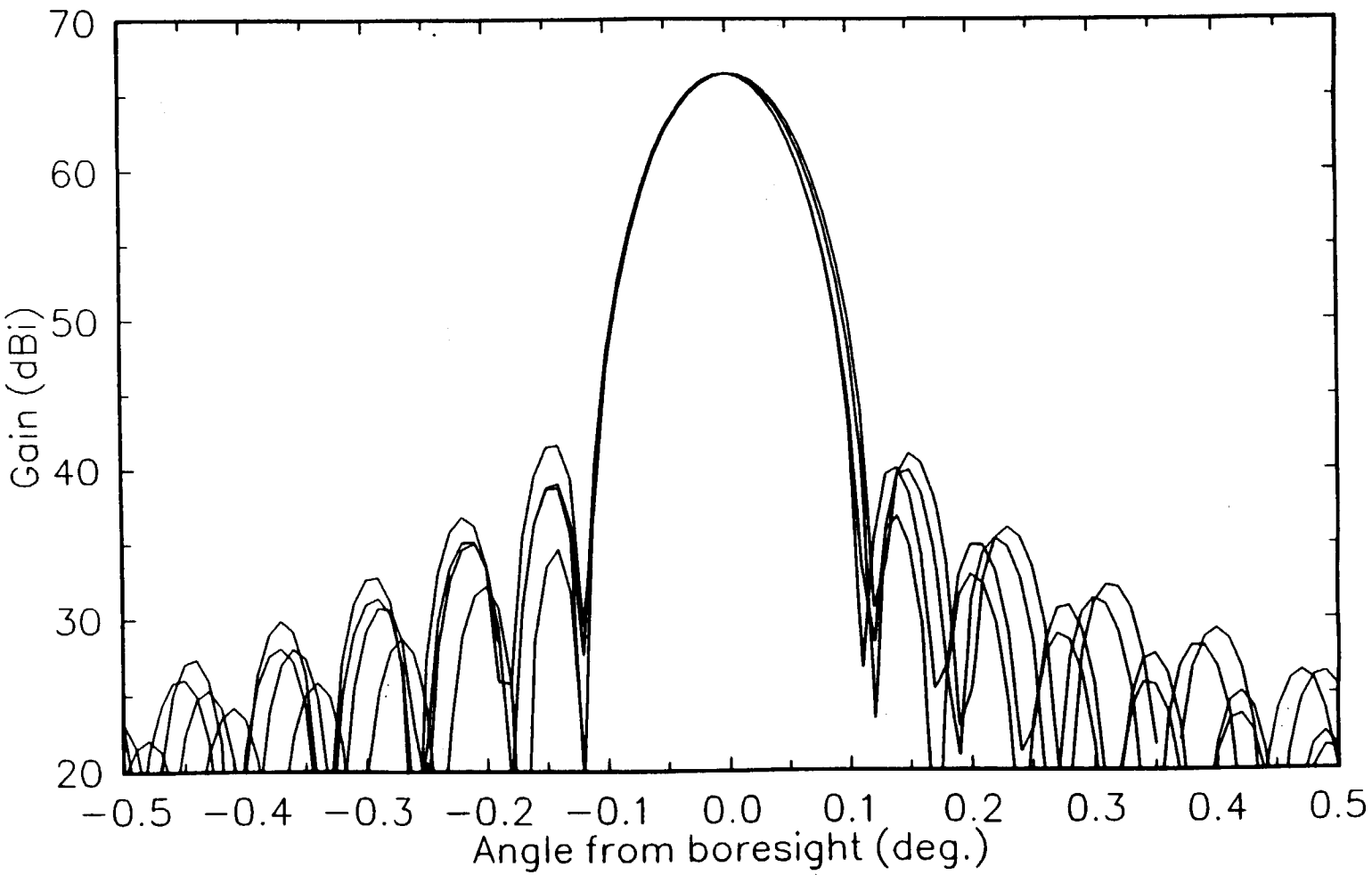

Figure 3.3-4 (d). Type 6 reflector antenna system - 10.7 m, 23.36 GHz, $\phi = 90^{\circ}$, $\theta = 0.5^{\circ}$.

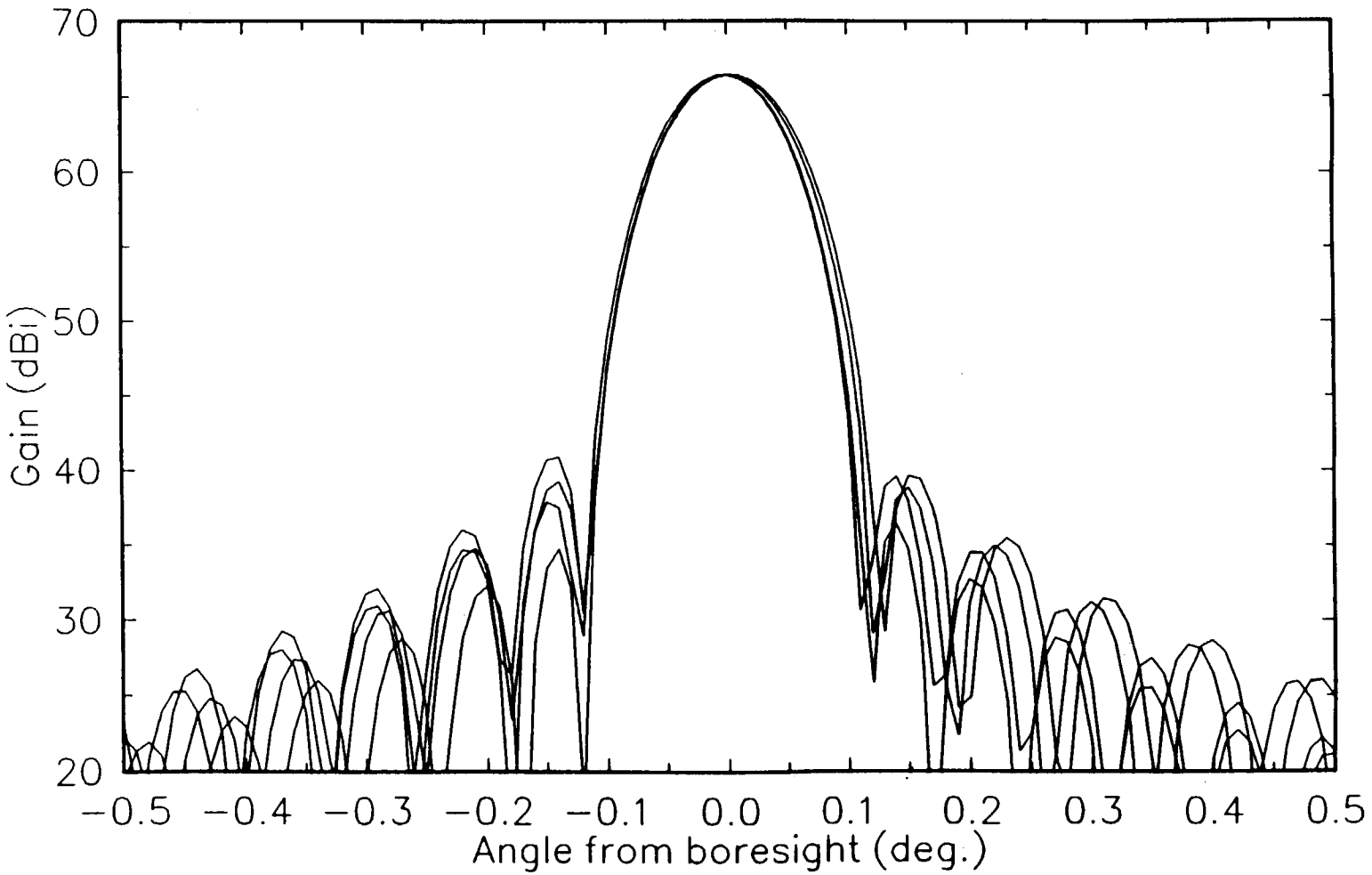

Figure 3.3-4 (e). Type 6 reflector antenna system - 10.7 m, 23.36 GHz, $\phi = 135^{\circ}$, $\theta = 0.5^{\circ}$.

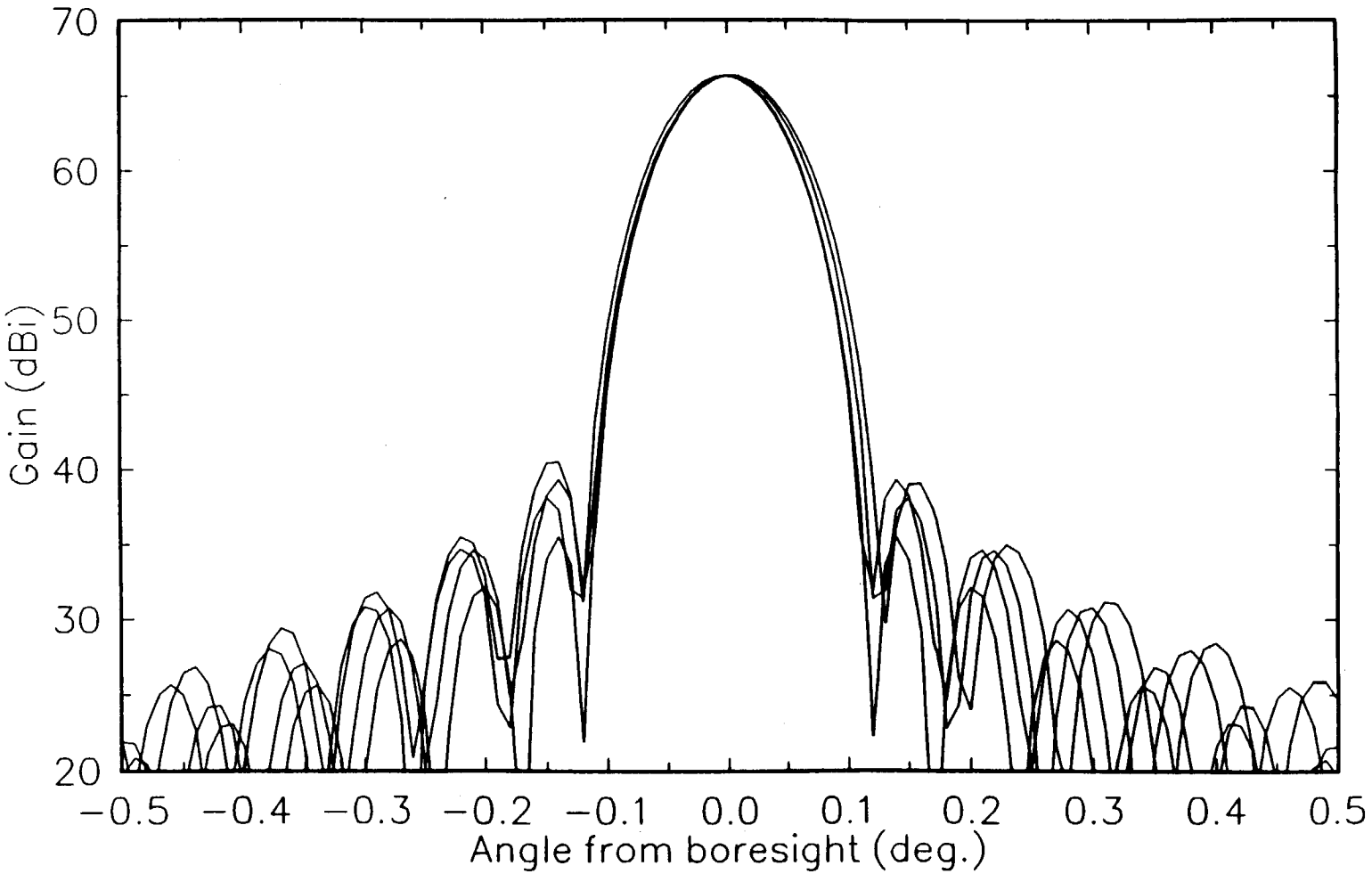

Figure 3.3-4 (f). Type 6 reflector antenna system - 10.7 m, 23.36 GHz, $\phi = 180^{\circ}$, $\theta = 0.5^{\circ}$.

4. A NEW SPHERICAL MAIN REFLECTOR SYSTEM DESIGN

4.1. Introduction

Spherical reflectors have excellent potential for wide scanning of a narrow beam pattern without main reflector motion. However, they are not commonly used because of poor aperture efficiency, high cross polarization and high side lobe levels. A new configuration has been developed which does not require oversizing the spherical main reflector to permit scan, thereby maintaining good aperture illumination. High aperture efficiency is achieved with low cross polarization and low sidelobe levels.

4.2. An overview of our new approach

The configuration consists of an offset spherical main reflector, a subreflector, and a tertiary reflector as shown in Fig. 4-1. The key to our approach is the synthesis of axially symmetric suboptics reflector shapes that provide a mapping from an isotropic feed pattern to a uniform distribution in the aperture plane as well as spherical aberration correction. Figure 4-2 shows a profile of the synthesized geometry. Scan is accomplished by rotating the sub-optics assembly along the R/2 sphere centered on the main reflector's spherical center, while tilting the feed to illuminate the same part of the main reflector. This unique feature of a constant illuminated portion of the main reflector eliminates the need for an oversized reflector which is common among scanning spherical reflector systems.

The synthesis approach is a two step process as follows:

(1) First, an isotropic feed radiation pattern is assumed and the suboptics are shaped to both correct for aberration and to produce a uniform amplitude distribution in the aperture of the main reflector.

(2) Second, the isotropic feed is replaced with a real feed. A perfect one-to-one correspondence mapping exists between the feed pattern and the aperture distribution and consequently, the aperture distribution can be controlled by the feed pattern. For example, if the feed has a Gaussian pattern, the aperture distribution will be Gaussian as well.

The beam from the sub-optics assembly is always fixed along the z axis. Therefore, the output rays from the offset main reflector are also directed along the z axis. However, we choose the z axis associated with the (θ, ϕ) scan coordinates to be from the offset main reflector aperture center to the its spherical center O. The initial scan angle θ can be changed by turning the z axis around O. While changing the θ angle, the feed is tilted accordingly relative to the z' axis so that the main reflector illumination area does not move in the (θ, ϕ) scan coordinate. In doing so, the illumination area on the sub-reflector and tertiary will change. The suboptics are oversized to accommodate scan. On the

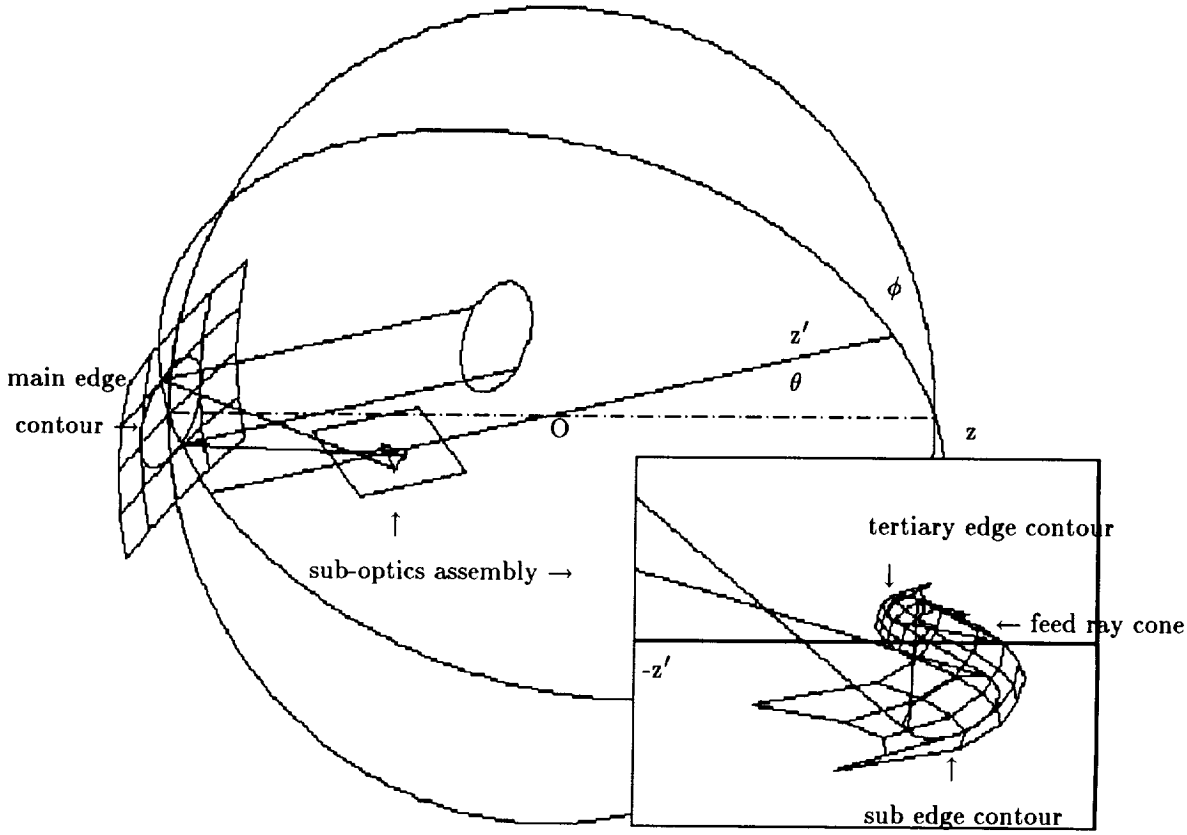

Figure 4-1. Configuration of the wide scanning spherical tri-reflector.

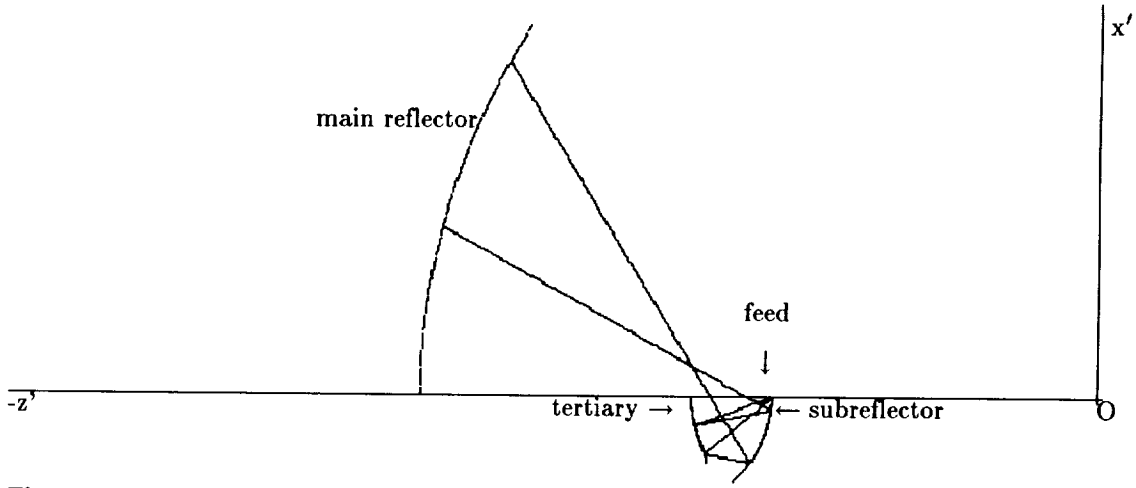

Figure 4-2. A profile of the synthesized spherical tri-reflector geometry.

other hand, keeping θ constant while rotating the z′ axis around the z axis offers another scan dimension (ϕ scan). Note from Fig. 4-1 that the sub-optics block is within the plane determined by z′ and z axes instead of being upright. Due to the symmetry of the main sphere, the scan in ϕ will not alter the optical properties of the system except the output ray direction.

Due to the sub-optics assembly geometry, only the scan in θ requires oversizing the sub-reflector and the tertiary. They are elongated in one dimension, but the sizes are not large. Furthermore, the arm holding the sub-optics assembly from the center of the sphere will naturally keep the assembly oriented in θ during ϕ-scan. So the mechanical motion is indeed simple.

4.3. Summary of three motions

There are three degrees of motion required to scan the main beam. Two degrees of motion determine the suboptics assembly location (as well as orientation) in the globally fixed scan coordinates. The third motion is the tilting of the feed within the suboptics assembly. These motions are described below.

(1) The suboptics assembly moves around main sphere center O. The suboptics assembly is held by an arm along a radius of R/2 from O. This arm should be able to move in both θ and ϕ directions as shown in Fig. 4-1. As the arm moves the suboptics assembly automatically keeps the θ-orientation as described in the previous section. In practice, this arm can be replaced by other mechanisms to reduce the length of the whole system.

(2) Feed motion within the suboptics assembly. The feed moves with the suboptics assembly. When θ-scan is performed (suboptics assembly moves in the θ direction), the feed has to be tilted relative to the suboptics z'-axis as shown in Fig. 4-1. This feed motion occurs only in one dimension (θ direction). Furthermore, if a fixed feed is desired, a beam waveguide can be used to create an image of the feed at the proper location in the suboptics assembly, and the reflected feed pattern can be tilted by a plane mirror. The design of the beam waveguide has also been studied.

4.4. Test Cases

Several calculations with G.O. synthesis code and GRASP7 analysis were performed. Feasible sizes of the system for the GEO design are summarized in Table 4-1. Although the subreflector and the tertiary are somewhat large, they occupy less than 10% of the mass of the main reflector. Furthermore, their sizes can be greatly reduced if the F/D can be increased. We are working on other alternatives to reduce the total length of the system.

PO analysis was performed using the GRASP7 code on a PC. Dual-caustic and single caustic test cases were investigated separately. In both cases, performance at three scan angles (both edges and the middle) over a 10° θ scan region were sampled. For each scan angle all the reflector edge contours were numerically defined from tracing the feed's edge ray cone. The reflector shapes were obtained by spline

interpolating the axisymmetric synthesis data into a regular grid. Test case results are given in Table 4-2.

Table 4-1

Spherical Tri-Reflector Design Configuration

Main reflector aperture diameter	25 m	
Sphere radius	62.5 m	
Total length of the antenna	<40 m	(no arm holding the suboptics from O)
Subreflector size	7.5 m × 4 m	(The edge is close to elliptical.)
Tertiary size	6 m × 4.25 m	(The edge is close to elliptical.)
Feed size	To be determined by -12 dB taper at ± 16°	

Table 4-2

Performance Results of Test Cases

	Dual-caustic case	Single-caustic case
Frequency	30 GHz	30 GHz
Main spherical reflector	D=5.7m, R=25m	D=10m, R=25m
Shaped sub-reflector	1.5m × 0.8m	3.0m × 1.6m
Shaped tertiary	0.7m × 0.2m (above z')	2.4m × 1.7m (below z')
Gaussian feed	-12 dB taper at ± 9°	-12 dB taper at ± 16°
Gain	63.2 dB	68.4 dB
Scan gain fluctuation	± 0.01 dB	± 0.01 dB
Aperture efficiency	65%	70%
Side lobe level	<-25 dB *	<-25 dB *
Cross polarization	<-40 dB *	<-35 dB *

* measured from the peak gain.

5. OPTIMIZATION OF REFLECTOR CONFIGURATIONS USING PHYSICAL OPTICS

5.1 Introduction

The geometrical optics (GO) is the most widely accepted technique used for the design of reflector antennas. An alternative method for reflector antenna synthesis is to use physical optics (PO) which accommodates specifications of the performance parameters in the synthesis process. Unfortunately, it is not possible to solve for reflector configurations directly from the physical optics based on a given feed pattern and a desired radiation pattern because it is not possible to invert the PO surface integral for an arbitrary reflector geometry. A technique to solve for the reflector configuration is to convert the problem to that of minimization. A functional which represents the difference between desired and calculated performance parameters can be defined and minimized using an iterative technique.

The code which implements the PO synthesis procedure is called Physical Optics Optimization Program (POOP). The program utilizes field correlation method (FCM) derived by Wood [1] based on the field correlation theorem. The theorem states that the aperture efficiency η of a surface S is given by the vector cross correlation of the received electric field $\vec{E}_r$ and the transmitted magnetic filed $\vec{H}_t$ over the surface S. Explicitly, η is given by

$$\eta = \frac{\left(\int_S \vec{E}_r \times \vec{H}_t^{\,*} \, ds \right)^2}{\int_S \vec{E}_r \times \vec{H}_r^{\,*} \, ds \int_S \vec{E}_t \times \vec{H}_t^{\,*} \, ds} \tag{5-1}$$

where the transmitted fields, $\vec{E}_t$ and $\vec{H}_t$, are electric and magnetic fields that exist over the reflector surface S when the antenna is fed by primary feed. The received fields, $\vec{E}_r$ and $\vec{H}_r$ are obtained by analyzing the antenna when the primary reflector is fed by a plane wave incident from a desired scan direction. The efficiency is maximum (η=1) when received fields and the transmitted fields are matched completely. The field correlation method uses the numerator of (5-1) to shape reflector surfaces. Specifically, the reflector surface S is modified by

$$\triangle = \frac{\lambda}{4\pi}\left(\angle \vec{E}_r + \angle \vec{H}_t^{\,*} \right) \tag{5-2}$$

where $\triangle$ is the change in the shape of reflector surface in wavelength and $\angle \vec{E}_r$ and $\angle \vec{H}_t^{\,*}$ are phase term of the received and the transmitted fields in radians and λ is the wavelength of the fields. The surface shaping is applied iteratively until maximum η is achieved.

5.2 Optimization of Foldes Type 6 Configuration

Initial optimization of Foldes Type 6 configuration based on GO is described. The Type 6 configuration is an offset Cassegrain dual reflector antenna with a limited scanning capability where scanning is accomplished by a combination of translation and rotation of subreflector. A detailed discussion of synthesis approaches for the Type 6 configuration are discussed in Chapter 3. Before reflector configurations can be optimized using PO, it is necessary to optimize the geometry using GO. In this section, effects of so called Mizuguchi's condition on the scan capability of Foldes Type 6 reflector configuration is discussed.

The Mizuguchi's condition was originally derived to minimize the cross-pol component of the far-field radiation in classical dual offset reflector configurations. [2] The condition species the tilt angle β between the major axis of hyperboloid/ellipsoid subreflector and the axis of the paraboloid main reflector and the feed tilt angle α from the major axis of the subreflector for a given eccentricity, e, of the subreflector. When the condition

$$tan\ \alpha = \frac{(e^2 - 1)sin\ \beta}{(e^2 + 1)\ cos\ \beta - 2e} \tag{5-3}$$

is satisfied, cross-pol radiation introduced by the asymmetry in the offset configuration is minimized. The condition is related to the equivalent paraboloid technique [3] which can be used to predict the far-field pattern of a classical dual reflector by a single equivalent paraboloidal reflector. The feed tilt angle α in the Mizuguchi's condition corresponds to the axis of equivalent paraboloid as shown in Fig. 5-1 for a Cassegrain configuration. The cross-pol due to asymmetry is minimized by pointing the feed towards the apex of parent equivalent paraboloid.

It is apparent that Mizuguchi's condition can introduce excessive spill over at the subreflector when offset distance of the equivalent paraboloid is large. Rusch, et al, have shown that an additional condition

$$tan\ \frac{\alpha}{2} = \frac{e-1}{e+1}\ tan\left(\frac{\beta - \theta_0}{2}\right) \tag{5-4}$$

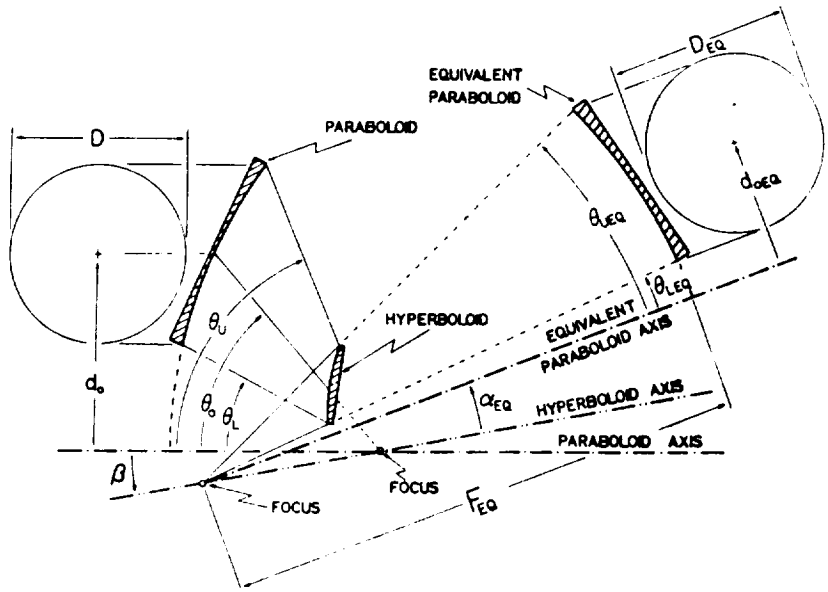

Figure 5-1. Equivalent paraboloid for the offset Cassegrain antenna [3].

can be imposed to minimize the spill over [3]. When the minimum spillover condition satisfied along with Mizuguchi's condition, the equivalent paraboloid becomes axisymmetric. It is well known that axisymmetric paraboloid has much better scan capability than a offset paraboloid when scanning is accomplished by lateral movement of the feed [4]. By satisfying the minimum spillover condition the scan capability of Type 6 configuration is also improved.

As an example consider two-dimensional Type 6 configuration for LaRC test article. The main reflector is a cylindrical parabola with focal length F=13.5 meters and offset height H=7.75 meters as shown in Fig. 5-2. The angles α and β are chosen such that all three cases have same equivalent focal length, F_{eq}=49 meters but with different equivalent offset heights: 1) H_{eq}=0 meter, 2) H_{eq}=5 meters and 3) H_{eq}=−5 meters. The case 1 satisfies Mizuguchi's condition as well as the minimum spillover condition. In the cases 2 and 3 only Mizuguchi's condition is satisfied.

Figure 5-3 shows the maximum gain vs scan angle when scanning is accomplished by feed displacement. The effects of axisymmetric equivalent parabola can be observed in three places in the gain curve. First, the gain value is higher at and near boresight for axisymmetric case which is due to less spillover at the subreflector. Second, the scan loss for the case 1 is close to symmetric about bore sight. Third and most import effect is that case 1 has wider scan range for a given scan loss.

Figure 5-4 shows the maximum gain vs scan angle when scanning is accomplished by translation and rotation of the subreflector. It is observed that the gain value for the case 1 is higher than the cases 2 and 3 over the $\pm$ 1.5 scan range. Unlike the cases for the scanning by feed displacement the case 3 has smaller scan loss than cases 1 and 2.

5.3 Application of PO Optimization

Shaping the reflector surface of Foldes Type 6 configuration using physical optics was investigated. The reflector configuration that satisfies both the Mizuguchi's condition and the minimum spillover condition is used as the initial geometry. Figure 5-5 shows the required translation and rotation of the subreflector for scan directions between -1.5° to $+1.5^\circ$ in 0.1° increments. It is apparent that the subreflector motions required within $\pm 1.5^\circ$ scan range can be modeled by linear functions which are also shown in Fig. 5-5. Figure 5-6 shows the difference between the required shape of main reflector and the original parabolic reflector shape. The synthesized shape is obtained by taking the average of required main reflector surface for scan directions between -1.5° to $+1.5^\circ$ at 0.1° increments. The result shows that the amount of shaping required is small (less than 0.4 mm at λ=3 mm for a frequency of 10 GHz). The small amount of shaping occurs for two reasons. First, the required shaping for the positive scan angles cancels the required shaping for the negative scan angles. Secondly, there are not enough degrees of freedom allowed for shaping of the main reflector. In order to increase the scan range of the Foldes Type 6 configurations, it is necessary to either increase the

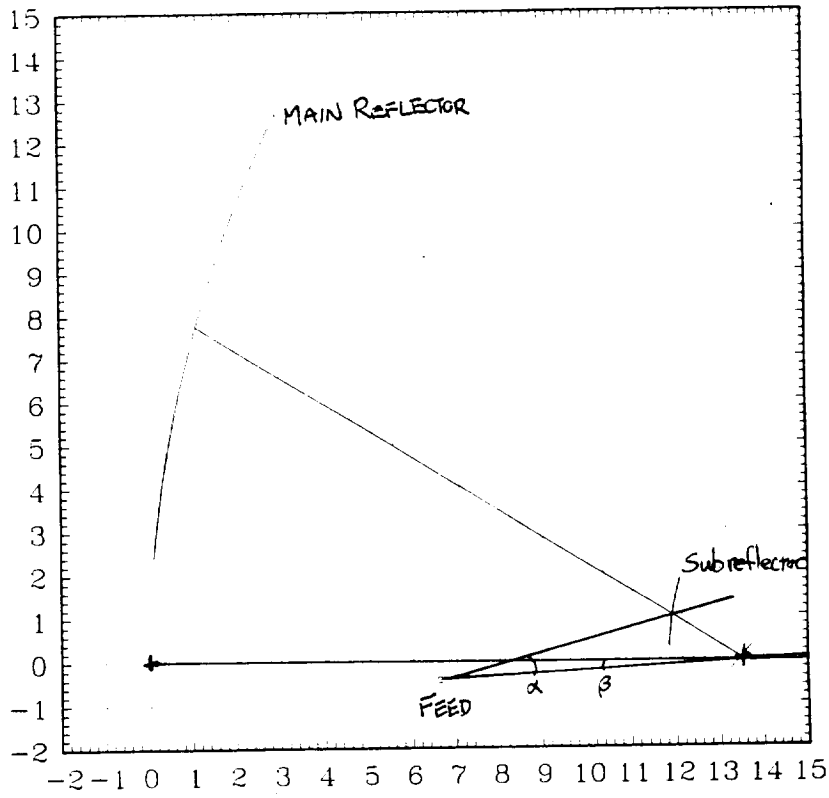

Figure 5-2. Foldes Type 6 reflector antenna that satisfy both Mizuguchi's condition and minimum spill over condition.

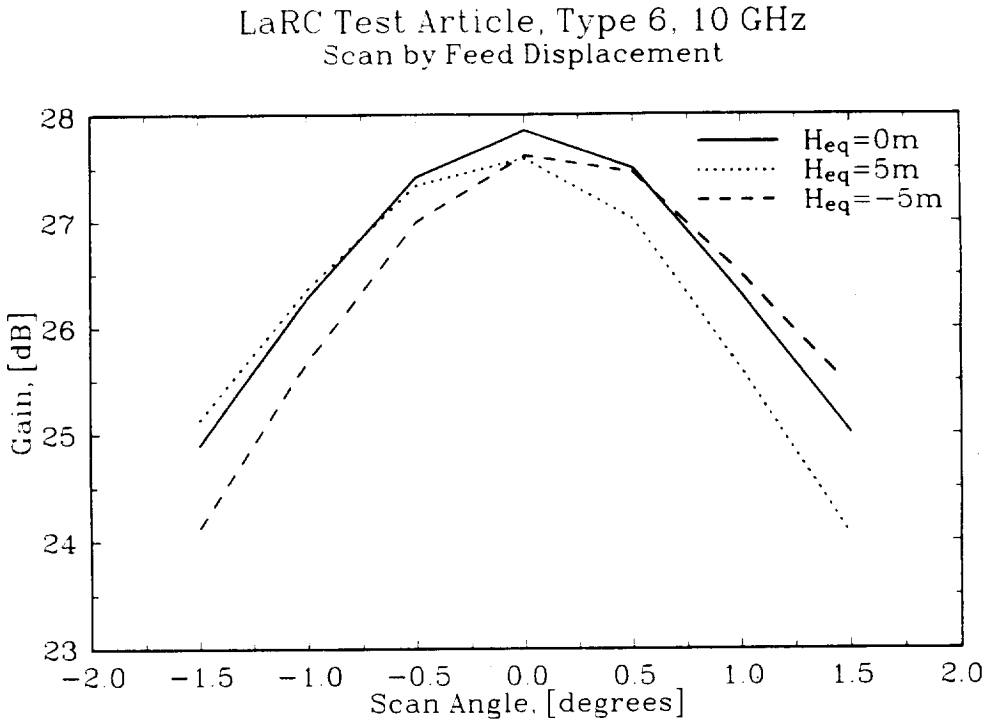

Figure 5-3. Gain vs scan angle of a classical Cassegrain system when the main beam is scanned by feed displacement.

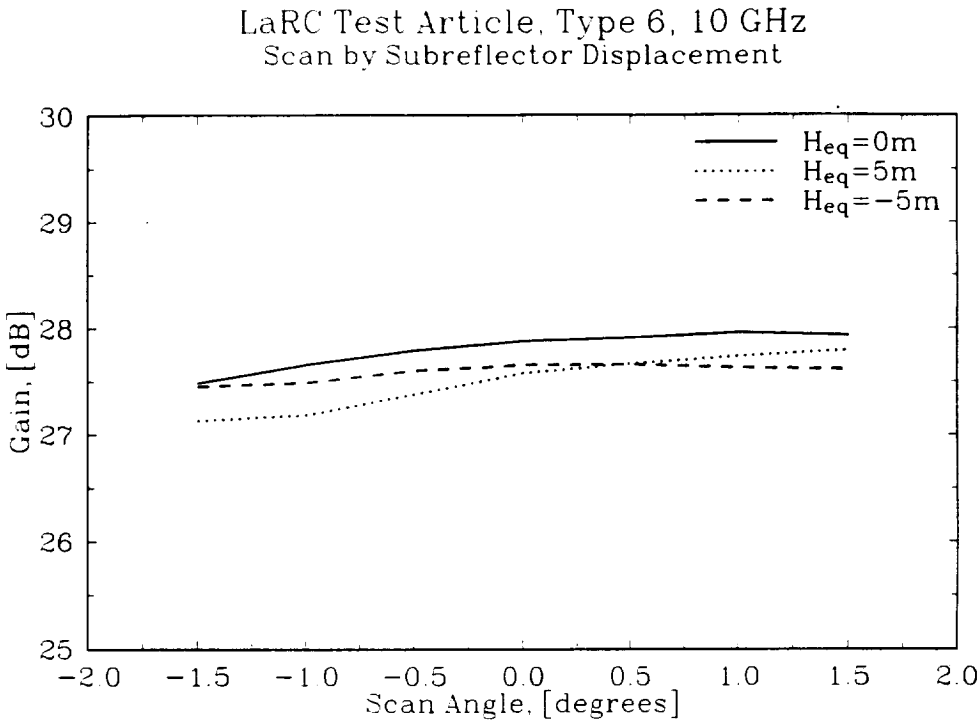

Figure 5-4. Gain vs scan angle of Foldes Type 6 configuration.

main reflector diameter or increase the subreflector diameter. When reflector sizes are allowed to increase, then different portions of the reflector surface can be illuminated for each scan direction.

5.4 Conclusions and Future Work

The effects of Mizuguchi's condition to the scan capability of Foldes Type 6 configurations were evaluated. In the Foldes Type 6 configuration, Mizuguchi's condition increases maximum gain over the scan range. The minimum spillover condition, however, does not necessarily minimize the scan loss. Shaping of the main reflector was also considered to increase the scan range of Foldes Type 6 configurations. It was shown that the system does not have enough degrees of freedom to allow significant improvement in scan capability of the system. Investigation of shaping Foldes Type 6 configurations with slightly oversized reflectors should be conducted in the future.

Further investigation into scan loss of Type 6 reflectors is proposed as a function of the following: angles α and β, the eccentricity, interfocal distance of subreflector, and offset height of the equivalent paraboloid.

5.5 References

[1.] P.J. Wood, *Reflector Antenna Analysis and Design*, Peter Peregrinio: London, 1980.

[2.] Y. Mizugutch, M. Akagawa and H. Yokoi, "Offset dual reflector antennas," *IEEE Antennas Propagat. Soc. Symp. Dig.*, pp. 2-5, Amherst, MA, Oct. 1976.

[3.] W. V. T. Rusch, A. Prata, Y. Rahmat-Samii and R. A. Shore, "Derivation and application of the equivalent paraboloid for classical offset Cassegrain and Gregorian antennas," *IEEE Trans. Antennas Propagat.*, Vol. 38, pp. 1141-1149, August 1990.

[4.] J. Ruze, "Lateral-feed displacement in a paraboloid," *IEEE Trans. Antennas Propagat.*, Vol. AP-13, pp. 660-665, Sept. 1965.

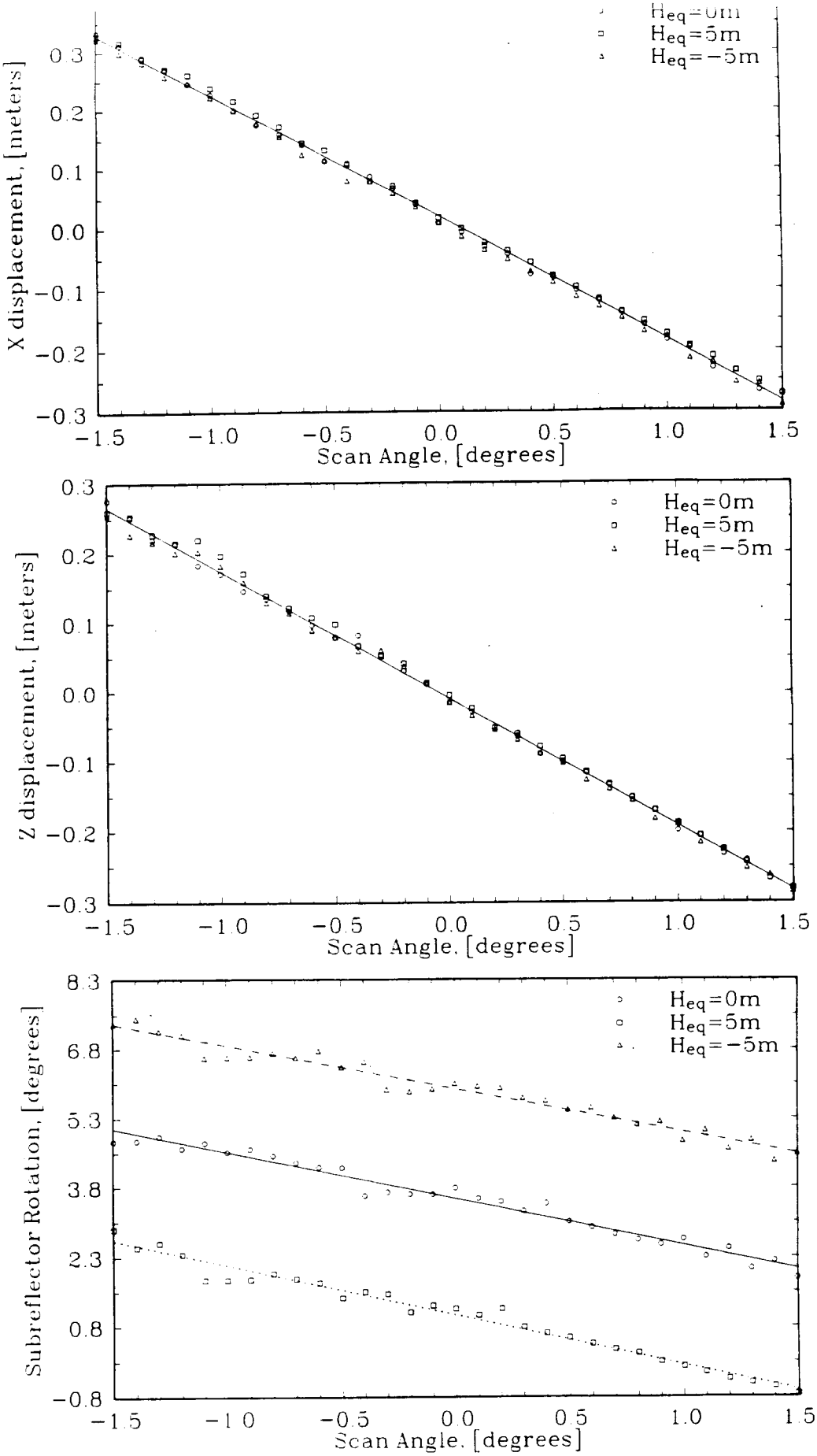

Figure 5-5. Required translation and rotation of subreflector in Foldes Type 6 antenna. a) X translation, b) Z translation, c) rotation.

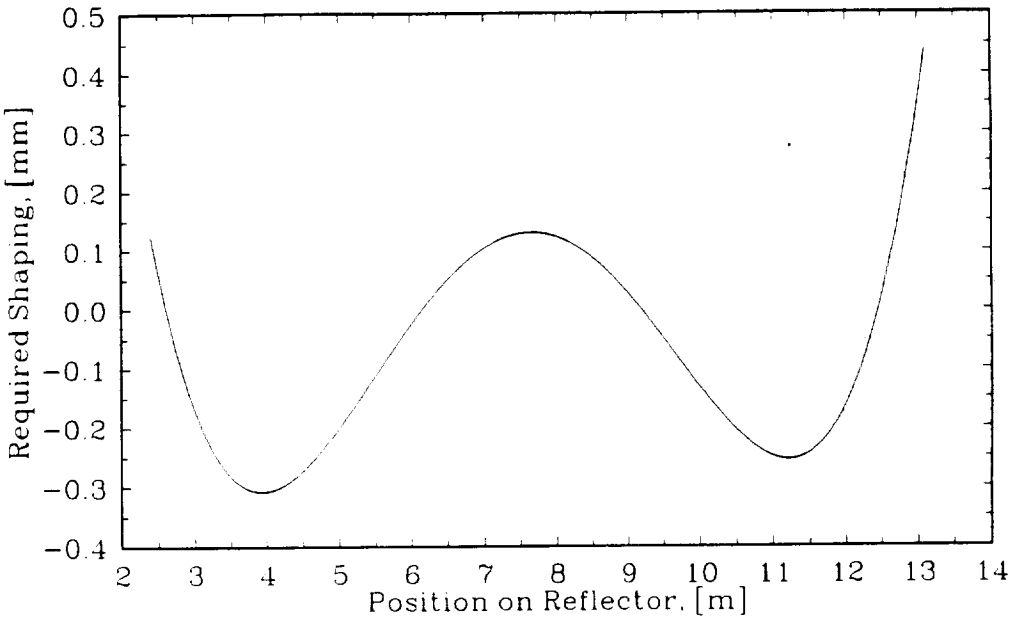

Figure 5-6. Required average shaping of main reflector obtained by physical optics optimization. The averages are taken for scan directions between $\pm 1.5^{\circ}$ at 0.1° increments.

6. RADIOMETRIC ARRAY DESIGN

This effort is funded under NASA Graduate Student Researchers Program Training Grant NGT-50413. A semi-annual report for that project has just been submitted as a separate document. This section summarizes the work on this effort.

In the development of new reflector scanning concepts the use of a feed array for beam steering and surface distortion correction has not received intensive investigation. While the design of arrays for communications applications is well developed, their use in remote sensing applications has not been studied extensively. This effort is directed toward developing modeling and analysis approaches for radiometric applications.

Previously, we developed a generalized analytical model to characterize the effects of noise contributions from the array, the feed network, and receiver. This model was based on network scattering parameters and estimated the total noise power measured at the receiver. One of the highlights of this model was the inclusion of mutual coupling, feed coupling, and mismatching effects on the received noise. For a passive network, all noise sources could be determined from the network scattering parameters. The noise characteristics of active devices must be supplied.

The network noise model we developed describes the external noise scene only as noise voltages impressed at the array elements. This is a very simplistic model since the interaction between the array and the external noise scene is quite complicated. It is not sufficient for characterization of an extended noise source to know just the voltages at the terminals of each array element. The correlation between elements must also be known. For extended incoherent noise sources interelement correlation can be derived from the spatial coherence function of the source. This however implies knowledge or assumption of the brightness distribution of the source.

The mutual coherence function (MCF) can be found analytically for simple noise sources assuming a brightness distribution across the source. The relationship between the source brightness distribution and the MCF is analogous to that between the aperture illumination of an antenna and its radiation pattern. That is, the brightness distribution of an incoherent source and its corresponding MCF are related by a Fourier transform. Thus, in order to calculate the MCF for an array imaging a noise source, it becomes necessary to postulate the form of the brightness distribution across the noise source. However since, in general, the size of an array will be relatively small when viewed from the source, errors due to an incorrect assumption of the source brightness distribution will be relatively small.

Using simple models for the brightness distribution of the earth, we have examined expected values of the MCF for remote sensing from both low-earth orbit and geostationary orbit. Results indicate that from low-earth orbit typical inter-element spacings (i.e. $> \lambda/2$) the MCF is zero. This

implies that the cumulative noise power received by each array element is incoherent with respect to the other elements. This simplifies the modeling of remote sensing arrays for low-earth orbit. For an array in geostationary orbit the MCF is not zero between elements but varies depending on the spacing between pairs of array elements. This results in a complication of the noise modeling of geostationary arrays.

Based on the results above we are pursuing models for calculating received noise from an earth-like target by an array. Efforts are initially concentrating on the low-earth orbit case since it is analytically the simplest. We will continue to pursue the modeling of arrays in geostationary orbit as our study if partial coherence theory continues.

7. BEAM EFFICIENCY STUDIES

A problem which arises in evaluating beam efficiency is the definition of the "main beam". Several different methods have been proposed to define the main beam of an antenna pattern. A study of beam efficiency is ongoing. Each proposed definition will be examined with emphasis on determining the most suitable definition of beam efficiency for GEO and LEO applications. This investigation will factor in the actual conditions of asymmetric patterns and ill-defined pattern nulls.

A large antenna is required for adequate earth surface resolution. Large antenna structures will have imperfect surfaces. The effects of antenna surface errors on beam efficiency impacts antenna performance. Classification of reflector surface errors is often based on characteristic correlation interval, C, for the phase errors in the aperture plane. These categories include random errors, radial periodic errors, azimuthal periodic errors, a combination of radial and azimuthal periodic errors, and combined periodic and non-periodic errors. A detailed study of each category of surface error will be undertaken, especially the effects of surface errors on antenna beam efficiency.

8. PUBLICATIONS

8.1 Recent Publications

8.1.1 Conferences

(1) P.C. Werntz, K. Takamizawa, W.L. Stutzman and P. Foldes, "Wide Scanning Tri-Reflector System with an Elliptic Subreflector and Moving Tertiary Reflector," URSI Radio Science Meeting (Boulder, CO), January 1992.

(2) R.M. Barts, W.A. Davis and W.L. Stutzman, "A Multiport Noise Model with Applications to Remote Sensing Arrays," URSI Radio Science Meeting (Boulder, CO), January 1992.

8.1.2 Papers

(1) W.T. Smith and W.L. Stutzman, "A Pattern Synthesis Technique for Array Feeds to Improve Radiation Performance of Large Distorted Reflector Antennas," IEEE Trans. on Ant. and Prop., Vol. 40, pp. 57-62, January 1992.

8.1.3 Theses, Dissertations, Reports

(1) W. Stutzman and G. Brown editors, "The Science Benefits of and the Antenna Requirements for Microwave Remote Sensing from Geostationary Orbit," NASA Contractor Report 4408, NASA Large Space Antenna Science Benefits Panel, 1991.

8.2 Planned Publications

8.2.1 Conferences

(1) P.C. Werntz, M.C. Bailey, K. Takamizawa and W.L. Stutzman, "Array-Fed Reflector Antenna Systems for Wide Scan," AP-S Symposium, July 1992.

(2) K. Takamizawa, P. Werntz, and W.L. Stutzman, "Optimization of Multiple Reflector Antenna Configuration for Wide Angle Scan," AP-S Symposium, July 1992.

(3) J. LaPean and W.L. Stutzman, "Beam Scanning in the Cassegrain Antenna System by the use of Subreflector Movement," AP-S Symposium, July 1992.

8.2.2 Papers

(1) J.W. LaPean and W.L. Stutzman, "Wide Scanning Dual Reflector Antennas Using a Moving Subreflector," to be submitted.

(2) K. Takamizawa and W.L. Stutzman, "Optimization of Multiple Reflector Antenna Performance Under Parameter Constraints," IEEE Trans. on Ant. and Prop., to be submitted.

(3) Shen and W.L. Stutzman, "Design of High Efficiency Reflector Antennas with Multiple Subreflectors for Wide Scan," to be submitted, July 1992.

(4) R.M. Barts and W.L. Stutzman, "Noise Modeling of Array Antennas with Applications to Microwave Remote Sensing," IEEE AP-S Trans., to be submitted 1992.

(5) P. Werntz and W.L. Stutzman, "Wide Scanning Tri-Reflector Antenna System Using Moving Tertiary Reflector," IEEE Trans. on Ant. and Prop., to be submitted.

8.2.3 Theses, Dissertations, Reports

(1) J.W. LaPean, "Beam Scanning in the Cassegrain Antenna System Using a Moving Subreflector," Master's Thesis, Virginia Tech, May 1992.

(2) K. Takamizawa, "Optimization of Multiple Reflector Antenna Performance Under Parameter Constraints," Ph.D. dissertation, Virginia Tech, August 1992.

(3) P.C. Werntz, "Novel High Gain Wide Scan Tri-Reflector Antennas," Ph.D. dissertation, August 1992.

(4) B. Shen, "Design of High Efficiency Spherical Reflector Antennas with Multiple Subreflector for Wide Scan," Ph.D. dissertation, August 1992.

(5) R.M. Barts, "Applications of Array Antennas to Microwave Remote Sensing," Ph.D. dissertation, August 1992.